UNIVERSITAT ROVIRA i VIRGILI

Copper-based hybrid nanomaterials for the electrocatalytic reduction of CO_2

Master's degree in Synthesis, Catalysis and Molecular design

2021-2022

Tarragona

Joan Marc Bondia Pedra

Supervised by Prof. Emilio Palomares and Dr. Federico Franco

Index

1. **ABSTRACT** 4
2. **OBJECTIVES** 5
3. **INTRODUCTION:** 5
4. **EXPERIMENTAL SECTION:** 13
   - 4.1. **Reagents and materials** 13
   - 4.2. **Synthesis of Cu_2O nanocubes (NCs):** 13
   - 4.3. **General synthesis of the hybrid materials:** 14
   - 4.4. **Electrochemical characterization and electrocatalytic tests** 16
5. **RESULTS AND DISCUSSIONS** 19
   - 5.1. **X-Ray Diffraction (XRD)** 19
   - 5.2. **Attenuated Total Reflection – Infrared (ATR-FTIR)** 20
   - 5.3. **Transmission Electron Microscopy (TEM)** 23
   - 5.4. **X-Ray Photoelectron Spectroscopy (XPS)** 29
   - 5.5. **Electrocatalysis** 31
     - 5.5.1. **Model molecular macrocyclic systems** 31
     - 5.5.2. **Cu_2O Nanocubes** 32
     - 5.5.3. **Cu_2O-based hybrid materials** 34
6. **CONCLUSIONS** 37
7. **ACKNOWLEDGEMENTS** 39
8. **BIBLIOGRAPHY** 40

1. ABSTRACT

Global warming and its consequences, the worldwide energy crisis and the issues related to increasing levels of carbon dioxide (CO_2) emissions in the atmosphere represent key challenges for modern society. These problems have prompted the research of new methods to transform CO_2 back to fuels and value-added chemicals. In this scenario, the electrochemical CO_2 reduction reaction (CO_2RR) powered by renewable energy sources has become an attractive sustainable approach to tackle this challenge. Nevertheless, an efficient catalyst is required to face the low selectivity, activity and the high overpotential of the process. Among the plethora of transition metal-based catalytic systems that have been explored so far for CO_2RR, copper (Cu)-based nanocatalyst have attracted increasing interest in the field over the last decades, due to their unique capability to promote an electrochemical reduction of CO_2 into multicarbon C_{2+} products.

In this work, we developed hybrid molecular-heterogeneous Cu-based nanomaterials for CO_2RR, with the aim of tuning the selectivity of the nanostructured Cu catalyst by the combination with a molecularly defined polymeric matrix. The design of these systems is based on a novel strategy, whereby cuprous oxide (Cu_2O) nanoparticles with a well-defined cubic geometry are used as both templates and catalysts for an *in-situ* polymerization based on azide-alkyne "click" reaction between the molecular building blocks. The resulting novel hybrid nanomaterials consist of an organic or metal-organic polymer layer surrounding the Cu_2O nanocubes, allowing to tune the electrocatalytic activity and selectivity of the copper catalyst.

2. OBJECTIVES

The aim of this research is the design of well-defined nanostructured cuprous oxide catalysts (Cu_2O) embedded into organic or metal-organic matrices by using Cu_2O nanoparticles with a well-defined shape and narrow size distribution as a template and as a catalyst for an *in-situ* azide-alkyne ‘’click’’ polymerization reaction. The novel hybrid materials were characterized by using spectroscopic and microscopic techniques, such as Attenuated Total Reflection (ATR), X-Ray Diffraction (XRD), X-Ray photoelectron spectroscopy (XPS), and Transmission Electron Microscopy (TEM). The purpose of the synthesis is to test these materials as catalysts for the electrochemical reduction of CO_2 using a H-type cell.

3. INTRODUCTION:

An increasing rate of carbon dioxide (CO_2) into the atmosphere, due to fossil fuel combustion and anthropic activities, results in several environmental issues, such us global warming, ocean acidification, melting of the polar ice and serious pollution problems.[1] Furthermore, the current energy crisis is forcing society to search for alternative methods to produce energy in a sustainable way. In this scenario, many research groups around the world have made great efforts to solve this situation, implementing new technologies to convert the CO_2 emitted by human activities to carbonaceous fuels and commodity chemicals, such as methane, ethylene, and ethanol among others, powered by renewable sources to achieve a new green economy.[2]

The electrochemical CO_2 reduction reaction (CO_2RR) powered by renewable energy is an attractive strategy to achieve this challenge. This approach allows to transform electrical into chemical energy, representing a sustainable way to produce commodity chemicals and/or liquid fuels, which can be widely employed in existing infrastructures.[3] Due to the high chemical stability of CO_2 molecule and the high energy barrier required for its activation,[4] a transition metal-based catalyst is generally required to reduce the overpotential and increase the reaction rate. Moreover, the catalyst design is essential to tune the CO_2RR selectivity towards the formation of some specific products. In this regard, the electrochemical CO_2 conversion relies on multiple proton and electron transfers steps, which potentially give rise to multiple mechanisms leading to a plethora of possible carbonaceous products (Table 1), depending on the type of catalyst and the external conditions.

In addition, the competitive hydrogen evolution reaction (HER) also represents another serious limiting factor which affects the overall faradic efficiency (FE) for CO_2RR, especially in aqueous media.

Reduction reaction	**Standard redox potential vs SHE (V)**
$CO_2 + 2H^+ + 2e^- \rightarrow CO + H_2O$	-0.52
$CO_2 + 2H^+ + 2e^- \rightarrow HCOOH$	-0.61
$CO_2 + 8H^+ + 8e^- \rightarrow CH_4 + 2H_2O$	-0,24
$2CO_2 + 12H^+ + 12e^- \rightarrow C_2H_4 + 4H_2O$	-0,34
$CO_2 + 6H^+ + 6e^- \rightarrow CH_3OH + H_2O$	-0,38

Table 1. *Possible CO_2 reduction pathways leading to carbonaceous products and corresponding standard redox potentials. Experimental conditions: pH 7 vs standard hydrogen electrode (SHE), 25ºC, 1 atm and 1M electrolyte.*[1]

Several families of organometallic complexes based on earth-abundant transition metals (e.g., Mn, Co, Ni, Fe) and nitrogen ligands, have been widely investigated as efficient catalysts for CO_2RR.[5-7] Compared to bulk heterogeneous materials, molecular catalysts are characterized by well-defined active sites, which make them ideal platforms to study in detail the structure-function relationship and the catalytic mechanism at a fundamental level.[8] They may operate as homogeneous catalysts in organic electrolytes or can be anchored onto solid electrodes by using a variety of immobilization strategies to perform CO_2RR in aqueous media. In terms of selectivity, CO and formic acid are the most common products formed by CO_2RR catalyzed by molecular systems. In particular, metal porphyrins are well-known to catalyze the CO_2 electroreduction to CO with high faradic efficiency. A commonly proposed general pathway for CO_2RR catalyzed by metalloporphyrins is based on an initial adsorption step of the CO_2 on the metal sites, followed by a protonation process, forming the *COOH intermediate, which is transformed to *CO by another protonation/reduction step and desorbed to form the CO product (Figure 1).[9]

Figure 1. *Proposed mechanism for electrochemical CO_2 reduction to CO by metal-porphyrins.*[9]

For instance, Daasbjerg et al. found that the cobalt-tetraphenylporphyrin (CoTPP) complex immobilized onto carbon nanotubes can efficiently catalyze a selective CO formation (FE >90%) at low overpotential in aqueous medium (Figure 2)**.**[10]

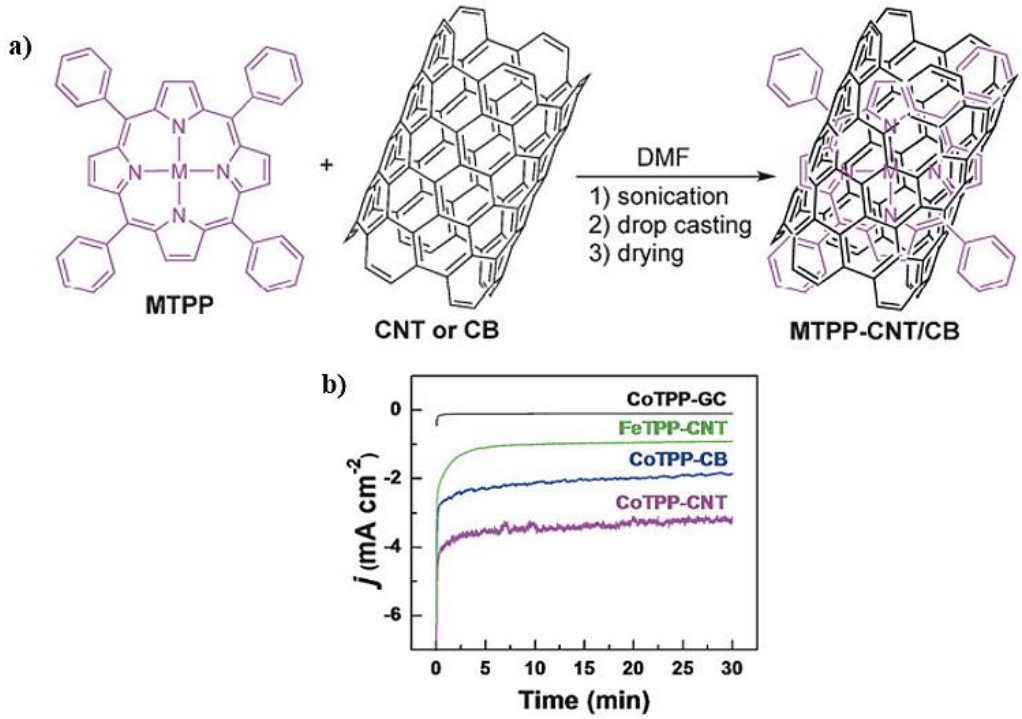

Figure 2. *a) Deposition of the metal-porphyrin on carbon nanotubes (CNT) or carbon black (CB) and b) current density recorded for 30 min of electrolysis at -1.35V vs SCE.*[10]

Moreover, in the last decades the group of M. Robert have reported a wide variety of iron porphyrin electrocatalysts for selective CO_2-to-CO reduction in non-aqueous homogeneous phase,[11-14] and as heterogenized on carbon electrodes in aqueous electrolyzers.[15] In particular, an Fe porphyrin substituted with trimethyl ammonium groups at the para position mixed with carbon black and deposited onto carbon paper support led high current densities for selective CO production (FE >98%) in a flow cell setup at low overpotential in neutral pH conditions.[16] The same group also implemented the use of carbon electrodes functionalized with cobalt phthalocyanine (Figure 3a) molecular catalyst as cathodes for an efficient CO_2RR to CO in flow cell electrolyzers (Figure 3b).[17]

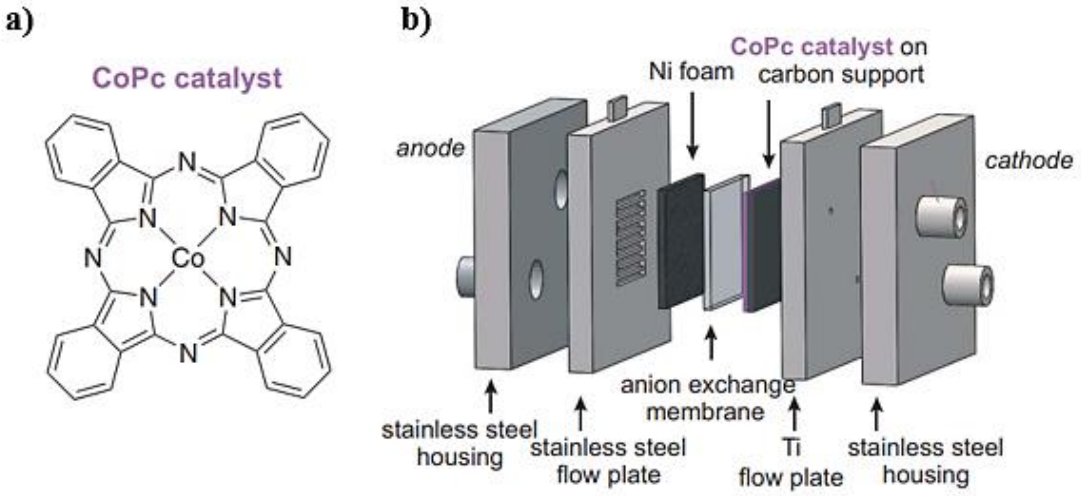

Figure 3. *a) Molecular catalyst used and b) Scheme of the flow cell, showing the cathode and anode GDEs.*[17]

In bulk heterogeneous catalysis, the catalyst usually contains a higher number of active surface states, without full structural control at molecular or atomic levels, generally obtaining high current densities at the expense of lower selectivity (Figure 4a).[2] Tremendous efforts have been put to improve catalytic behavior, controlling the shape, the size, and the morphology of the metal nanocatalysts.[18] The product distribution is determined by the relative adsorption energies of *CO, *COOH and *H intermediates (* indicates the active site for molecule adsorption on the metal surface) (Figure 4b).[19] In particular, the adsorption energy of the key *CO intermediate is commonly used as a general descriptor for CO_2RR selectivity of transition metal-based heterogeneous catalysts.[20] Whereas metallic surfaces featuring weak *CO binding tend to favor CO desorption and release, too strong CO adsorption inevitably leads to catalyst poisoning.

For intermediate values of *CO binding energies, the *CO intermediate may be stable enough to undergo successive electrochemical and/or chemical steps.[19]

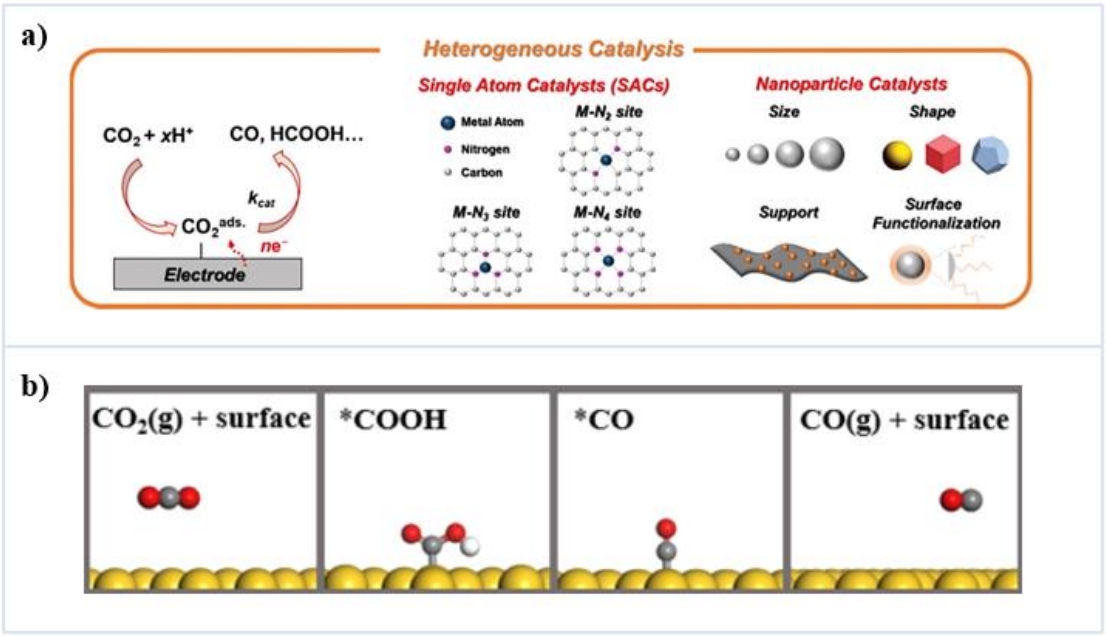

Figure 4. *a) Example of heterogeneous catalysis in CO_2 reduction[2] and b) mechanism proposed for CO_2 reduction to CO on Au surface.[18]*

In this regard, copper displays unique features among the other transition metals explored so far for CO_2RR, due to their capability to reduce CO_2 to C_{2+} products. Nevertheless, Cu based electrocatalysts are typically affected by high overpotentials and low selectivity, producing mixtures of several products, including ethylene (C_2H_4), hydrogen (H_2), methane (CH_4), carbon monoxide (CO), ethanol (EtOH), methanol (MeOH) among others.[21] However, understanding copper ability to produce hydrocarbons would help for the development of new catalysts active at lower potential with higher selectivity.[22]

The high overpotentials arises from the activation and binding energies of reaction intermediates. The catalytic surfaces have to bind *CO intermediates to produce the C-C coupling, which is critically dependent on the *CO coverage on the catalytic surface. Copper-based materials have unique electronic properties capable to bind the *CO intermediates strong enough to produce the C-C coupling without facing high activation barriers.[23] Moreover, DFT studies suggest that the (100) and (211) surfaces facets, predominantly in Cu_2O nanocubes (NCs), are more selective towards C_{2+} products[24,25] were the C-C coupling is favored.

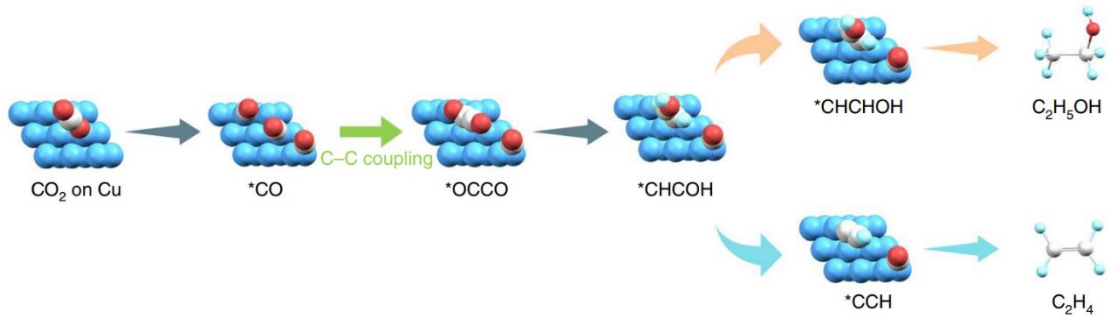

Figure 5. *Pathways for CO_2RR to ethanol and ethylene calculated using DFT methods.*[25]

Tuning the binding strengths of reaction intermediates has proven to be efficient to steer selectivity towards C_{2+} products like ethanol or ethylene. Doping Cu-based heterogeneous materials with silver, for example, led to increase the FE for C_2H_4 and C_2H_5OH formation reaching nearly 60 and 25%, respectively, by modulating the adsorption of key intermediates on the catalyst surface.[26] Furthermore, Cu-based bimetallic catalysts have shown to generate, a high concentration of *CO (key intermediate to produce C_{2+} products) on the doping sites, to spill over to the Cu surface to promote the C-C coupling. Sargent et al. have reported a hybrid molecular-heterogeneous composite material that produces a high concentration of CO due to the molecular adsorbate. DFT calculations suggested that the increased coverage of CO on Cu surface, decreases the reaction energy for the C-C coupling step and steers selectivity form ethylene to ethanol (Figure 5).[25] In other work, Zhuang et al. reported a method to enhance the C_{2+} products selectivity by enriching CO_2 molecules using a 50 nm film of polyaniline coating (PANI) on Cu nanoparticles, increasing the FE of C_{2+} hydrocarbons until the 80%, with a FE of ethylene over 40% at -1.1V vs RHE (Figure 6). An *in-situ* FTIR revealed that the increased CO coverage facilitates the C-C coupling on the Cu surface.[27] Furthermore, Sun et al. reported a Cu-based metal-organic framework (Cu-MOF) to form a coral-like shape containing metalloporphyrins. Supplying more CO intermediates on the Cu surface, they were able to reach an ethylene FE of 33.42% at -1.17V vs RHE using a Cu-based Fe-porphyrin, more than using the sole Cu catalyst (16,85% at -1.27V vs RHE**)**.[28]

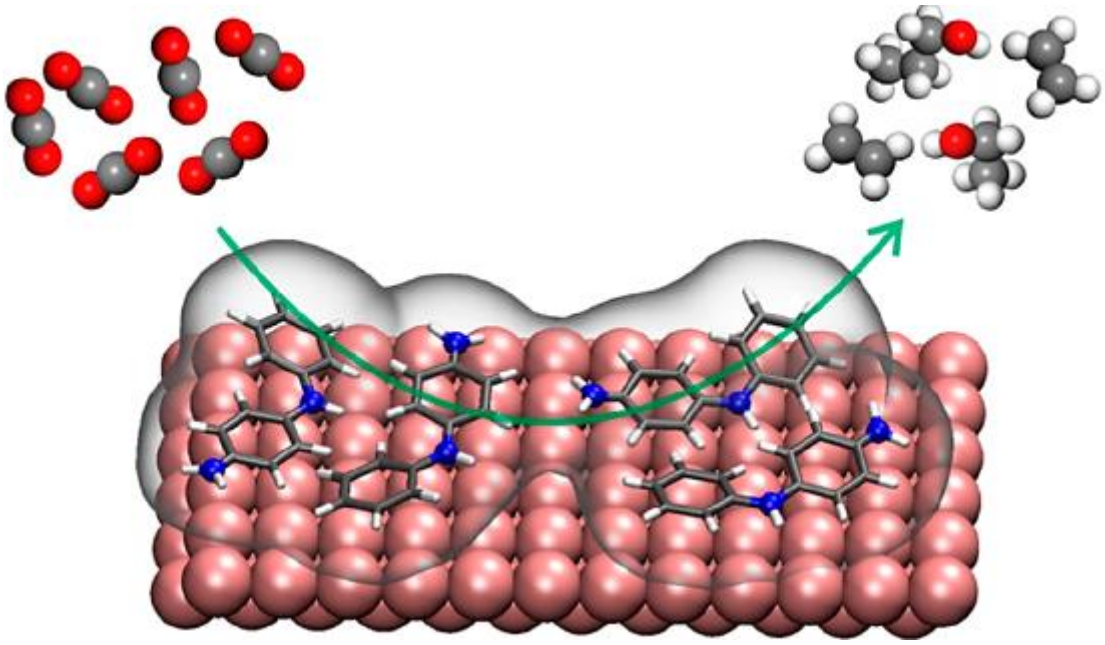

Figure 6. *50 nm polyaniline coating on Cu nanoparticles reducing CO_2 to hydrocarbons.*[27]

In view of these findings, this work presents a novel route to hybrid molecular-heterogeneous nanoreactors for tandem CO_2RR electrocatalysis. It is based on the combination of a CO-selective molecular catalyst with a copper-based nanocatalyst with the aim to enhance the surface CO coverage at the Cu surface, thus favoring the key C-C coupling step and improving the formation of C_{2+} products (Figure 7).

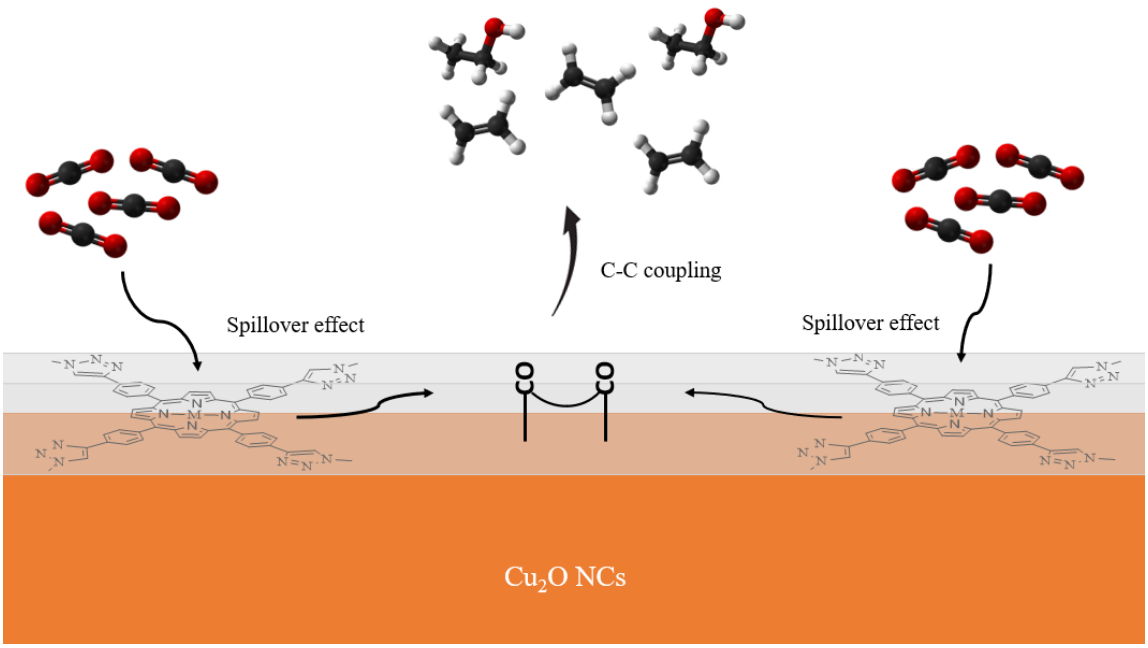

Figure 7. *Tandem CO_2RR catalysis performed by hybrid molecular-heterogeneous cupreous oxide nanocubes.*

In contrast with previous literature, the incorporation of molecular units to form the hybrid materials is not obtained by simple mixing or physical adsorption of the molecular component onto the nanostructured catalyst, but rather by growing a molecularly-defined polymer layer around the particle by using the latter as template and catalyst for the *in-situ* polymerization reaction. For this purpose, cubic Cu_2O nanoparticles were used to catalyze an azide-alkyne polymerization "click" reaction between organic or metal-organic building blocks bearing terminal ethynyl groups (including cobalt and iron porphyrin derivatives) and a multiple azide monomer to form a polymeric matrix under mild thermal conditions (Figure 8):

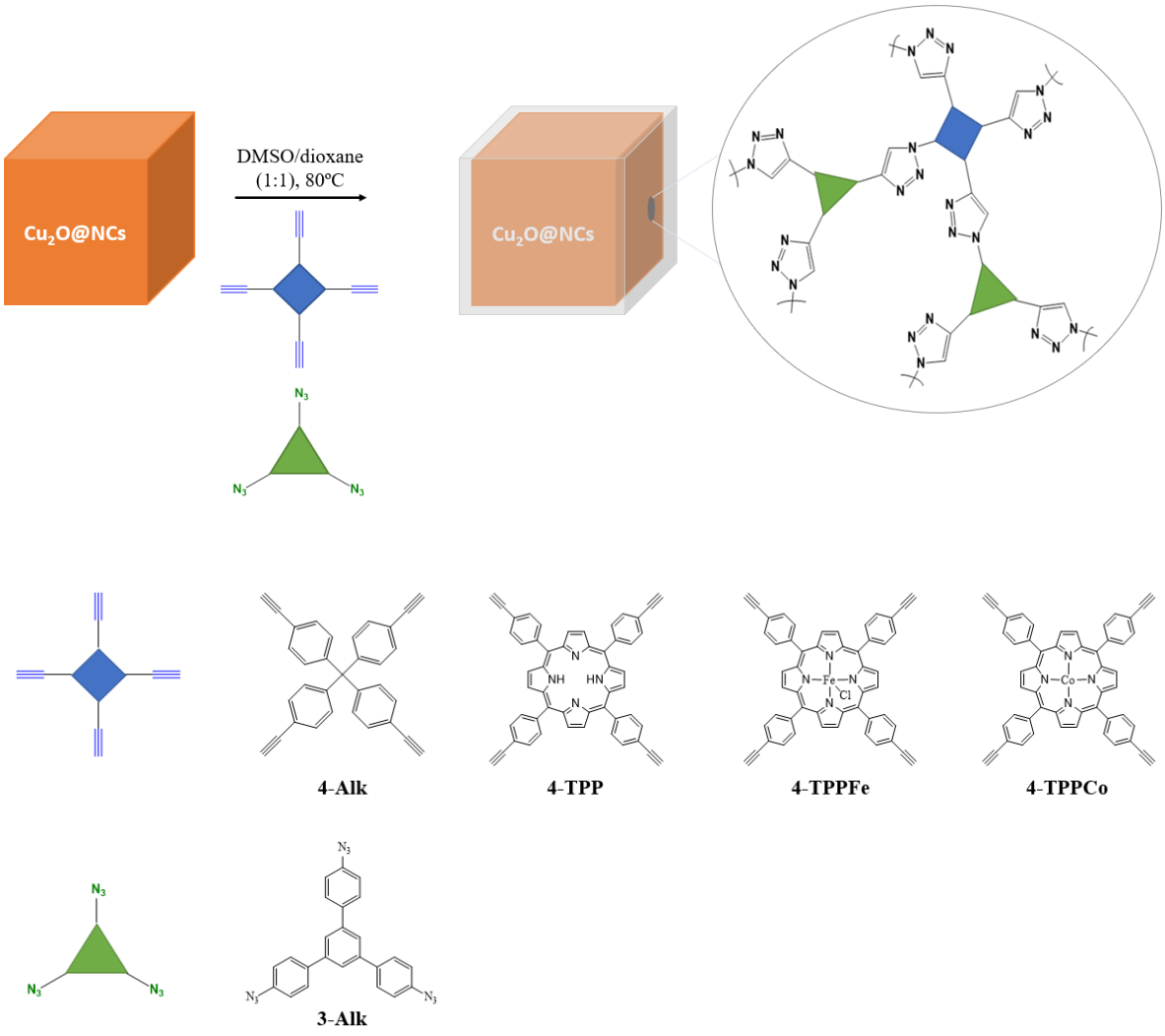

Figure 8. *Scheme of azide-alkyne cycloaddition catalyzed by Cu_2O nanoparticles, with the monomers used experimentally in this work.*

The 1,3-dipolar cycloaddition reaction of organic azides and alkynes has gained considerable attention recent years with Cu(I) catalysts due to its extreme robustness, simplicity, and substrate tolerance.[29] Similar systems have been reported, but they have never been tested to catalyze the CO_2RR.[30] These hybrid materials based on Cu_2O nanocubes surrounded by a metal-organic polymer are primarily designed with the aim to probe the CO spillover effect on a copper catalyst by using a molecularly-defined polymer. In addition to the catalytic tandem function, the metal-organic coverage may enhance the stability of the Cu_2O nanocube catalyst during electrocatalysis in aqueous media. Additionally, it may increase the hydrophobicity on the copper surface, thus preventing the adsorption of water molecules to the copper surface and disfavoring HER.

4. EXPERIMENTAL SECTION:

4.1. Reagents and materials

For the synthesis of Cu_2O nanocubes, commercially available reagents were employed: Trisodium citrate dihydrate **($C_6H_9Na3O_9$)**, copper (II) sulfate (**Cu_2SO_4**), sodium hydroxide (**NaOH**), L-ascorbic acid **($C_6H_8O_6$).** 5,10,15,20-(Tetra-4 ethynylphenyl)porphyrin (**4-TPP**), iron (III) 5,10,15,20-(tetra-4-ethynylphenyl)porphyrin chloride (**4-TPPFe**), cobalt (II) 5,10,15,20-(tetra-4-ethynylphenyl)porphyrin (**4-TPPCo**) were purchased by Porphychem and used as received. Tetrakis(4-ethynylphenyl)methane (**4-Alk**) was purchased by TCI, whereas 4,4''-diazido-5'-(4-azidophenyl))-1,1':3',1"-terphenyl (**3-N_3**) was synthesized according to reported literature.[31] Dimethyl sulfoxide (**DMSO**), dioxane, dichloromethane (**DCM**), diethyl ether (**Et_2O**), ethanol (**EtOH**), acetone.

4.2. Synthesis of Cu_2O nanocubes (NCs):

Cu_2O nanocubes (NCs) were prepared according to the synthetic procedures in the literature.[30] In a 500 mL Erlenmeyer flask, 2 mL of trisodium citrate dehydrate aqueous solution (0.9 M) was added to 400 mL of water. After 20 min stirring, 2 mL of $CuSO_4$ aqueous solution (1.2 M) was added to the solution. After 5 min stirring, 2 mL of NaOH aqueous solution (4.8 M) was added to the solution, which turned into deep color and became turbid. These changes are indicative of less soluble $Cu(OH)_2$ formation. After stirring for other 5 min, 2 mL of ascorbic acid aqueous solution (1.2 M) was added to the solution. A color change from blue to orange was observed due to the formation of Cu_2O (Figure 9). In this step is where the nucleation and growth of the nanoparticles occurs,

giving a yellow coloration to the solution due to the formation of small nanoparticles, and changing to orange due to the growth of the nanoparticles. After stirring for other 30 min, Cu_2O nanocubes were retrieved by centrifugation and washed with water, water:ethanol 1:1 solution and ethanol. The Cu_2O nanocubes were dried under vacuum.

Figure 9. *Experimental images relative to the synthesis of Cu_2O nanocubes. Color change from blue to orange, which corresponds to the evolution from Cu(II) species to Cu_2O NCs.*

4.3. General synthesis of the hybrid materials:

The Cu_2O-based hybrid materials were prepared according to the synthetic procedure in the literature.[32] Cu_2O nanocubes (70 mg) were added to a vacuum dried sealed vial or Schlenk flask. Under an inert Ar atmosphere, 15 mL of a mixture of DMSO/dioxane (1:1) were added to the vessel. The reaction mixture was further sonicated for 1h. Then, the corresponding alkyne and the 3-N_3 monomers (Table 2) were dissolved in DMSO/dioxane (1:1) (4 mL for each monomer) and added to the reaction mixture. After 10 minutes of bubbling the Ar in the mixture, the reaction was heated at 80ºC for 20 h maintaining the inert atmosphere with a balloon. After cooling the mixture at room temperature, the solid was retrieved by centrifugation and washed with DMSO, acetone, dioxane, DCM and Et_2O, and dried under vacuum.

Catalyst Nomenclature	Alkyne Monomer	Azide Monomer	Mg/mols of alkyne	Mg/mols of azide
Cu2O@4-Alk	4-Alk	3-N_3	3.16 mg 0.00759 mmol	4.35 mg 0.01012 mmol
Cu2O@4-TPP	4-TPP	3-N_3	5.39 mg 0.00759 mmol	4.35 mg 0.01012 mmol
Cu2O@4-TPPFe	4-TPPFe	3-N_3	6.08 mg 0.00759 mmol	4.35 mg 0.01012 mmol
Cu2O@4-TPPCo	4-TTPCo	3-N_3	5.83 mg 0.00759 mmol	4.35 mg 0.01012 mmol
Cu2O@4-TPPCo+	4-TTPCo	3-N_3	17,49 mg 0.02278 mmol	13,05 mg 0.03038 mmol

Table 2. *Experimental amounts of monomers used for each catalyst and their nomenclature.*

4.4. Electrochemical characterization and electrocatalytic tests

The electrochemical measurements were carried out using a BioLogic potentiostat (SP-150) in a custom-made two-compartment H-type cell, in which the working and counter electrode were separated by an anion-exchange Selemion AMV membrane (AGC Engineering) (Figure 10). In a typical experiment, 18 mL of electrolyte (0.1M $KHCO_3$) were added to each compartment. Before the electrochemical reaction, the electrolyte was purged for 30 minutes with a constant flow of CO_2 (30 mL/min), regulated by mass flow controllers (Alicat). A constant flow of CO_2 (30 mL/min) was also maintained during the whole electrolysis experiment.

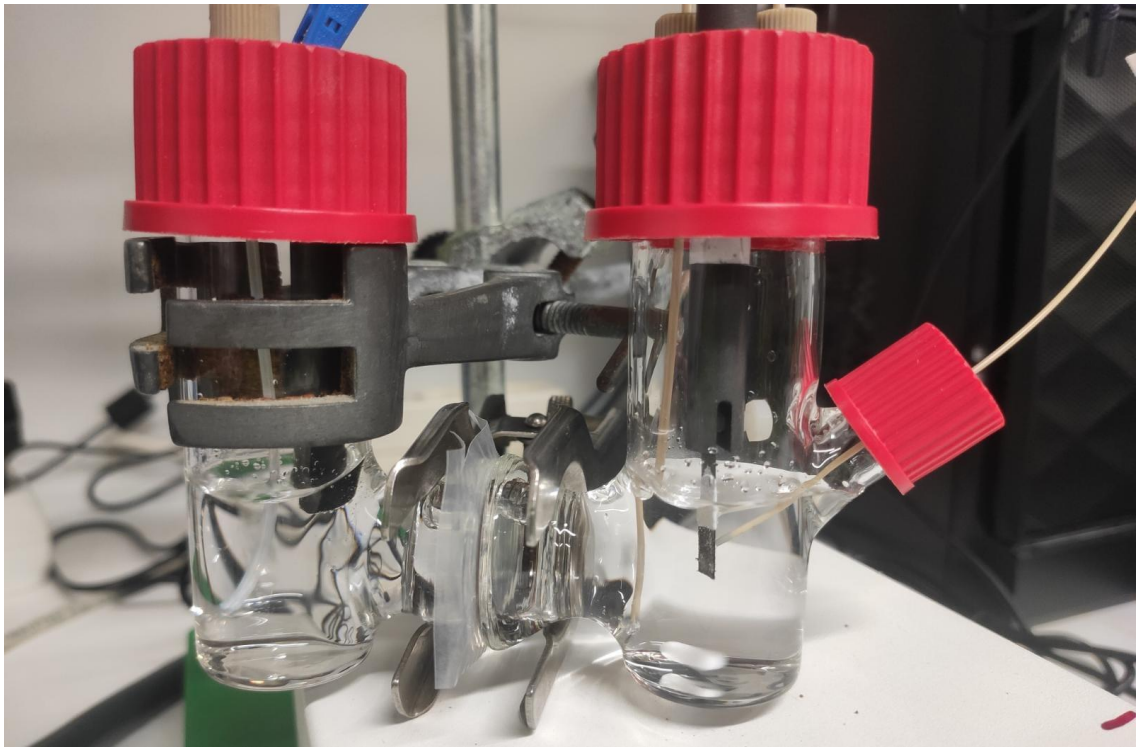

Figure 10. *Custom-made H-type cell. The cathodic compartment and anodic compartment are separated by an anion exchange membrane.*

The cathodic compartment outlet was connected to an online Agilent GC gas chromatograph where the gas products were analyzed (Figure 11).

A carbon rod (XRD Graphite Manufacturing Co., Ltd) was used as counter electrode (CE), whereas a leak-free Ag/AgCl electrode (Alvatek) was used as a reference electrode. The potential values are converted vs. Reversible Hydrogen Electrode (RHE), according to the following equations:

$$E(V \text{ vs RHE}) = E(V \text{ vs. Ag/AgCl}) + 0.059 \cdot pH + 0.197 \qquad \textit{(equation 1)}$$

The catalyst ink was prepared by dispersing 2 mg of nanoparticles in 950 µL of absolute ethanol. After sonication for 30 minutes, 50 µL of Nafion solution were added and the suspension was further sonicated for other 10 minutes. The working electrode (WE) was prepared by drop casting 25 µL of the catalyst ink onto carbon paper Toray TGP-60 (0.5 cm^2, Alfa-Aesar). For each measurement, a freshly prepared electrode was used to avoid influences of adsorbates or catalyst changes.

For testing the model molecular systems, such as the Cobalt phthalocyanine (CoPc) and the Cobalt tetraphenylporphyrin (CoTPP) supported on multi-walled carbon nanotubes (MWCNT), reported procedures were adopted for the electrode preparation.[33] For the preparation of CoPc/MWCNT electrode, 3 mg of MWCNTs were first dispersed in 2 mL ethylene glycol (EG)/ethanol (EtOH) 1:1(v/v) mixture followed by 30 min of sonication.

In a separate vial, 1 mg of CoPc (Alfa Aesar) was dissolved in 1 mL EG/EtOH mixture and 200 µL of the mixture was added to the MWCNTs suspension. After increasing the total volume of this solution to 3 mL and further 30 minutes sonication, 18 µL of Nafion solution was added to the mixture. The catalyst ink, obtained by further 30 minutes sonication, was finally drop-casted (100 µL) onto carbon paper Toray TGP-60 (0.5 cm^2, Alfa-Aesar). For the fabrication of the CoTPP/MWCNT electrode, 5 mg of CoTPP (STREM) were mixed with 5 mg of MWCNTs in 950 µL of EtOH.[10] After 30 minutes sonication, 50 µL of Nafion was added to the mixture. The catalyst ink, obtained by further 30 minutes sonication, was finally drop-casted (25 µL) onto carbon paper Toray TGP-60 (0.5 cm^2, Alfa-Aesar).

All the electrochemical experiments started with a linear scan voltammetry (LSV), performed with a scan rate of 10 mV/s from the open circuit potential (OCP) to the electrolysis potential. Then, a chronoamperometric experiment was performed for 100 minutes at constant applied potential.

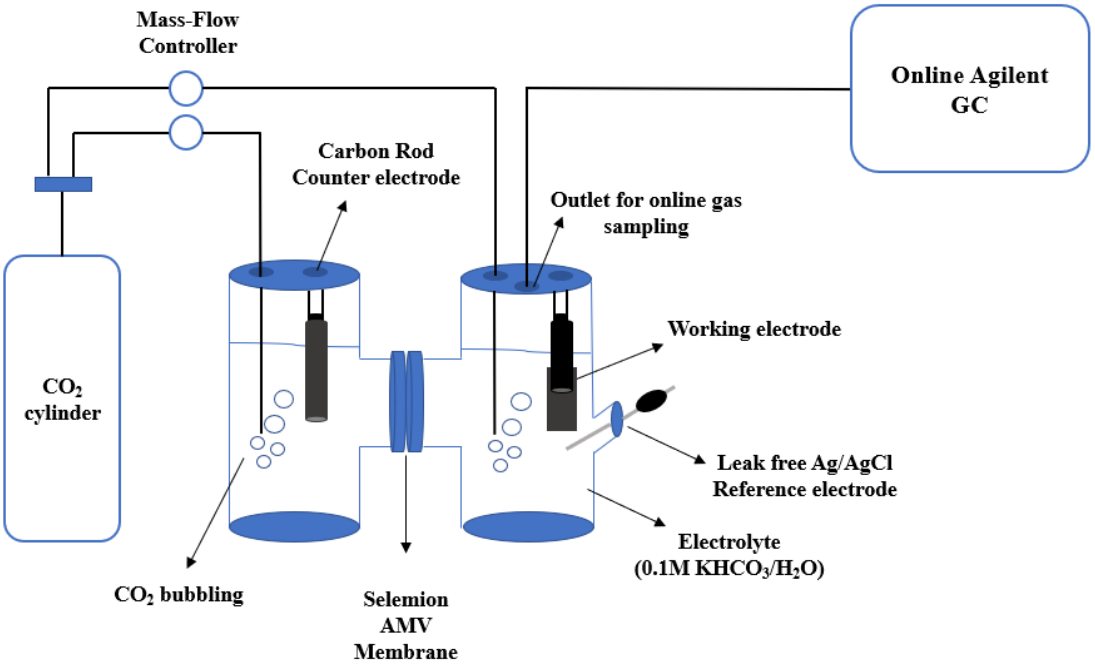

Figure 11. *Scheme of the set up used for the electrochemical performance.*

The cathodic compartment outlet was connected to an online Agilent GC gas chromatograph where the gas products were analyzed (Figure 11). A quantitative analysis of the gas phase evolved at the cathode during the electrocatalytic test was carried out by online gas-chromatographic measurements at regular time intervals (22 minutes). An Agilent GC-7890 instrument was used, equipped with two columns (Pore-PLOT, Molesieve-5A) and two detectors (FID, TCD).

5. RESULTS AND DISCUSSIONS

5.1. X-Ray Diffraction (XRD)

The powder X-Ray diffraction technique is used as a primary screening method and provides fundamental information about different crystalline form analyzed of each sample.

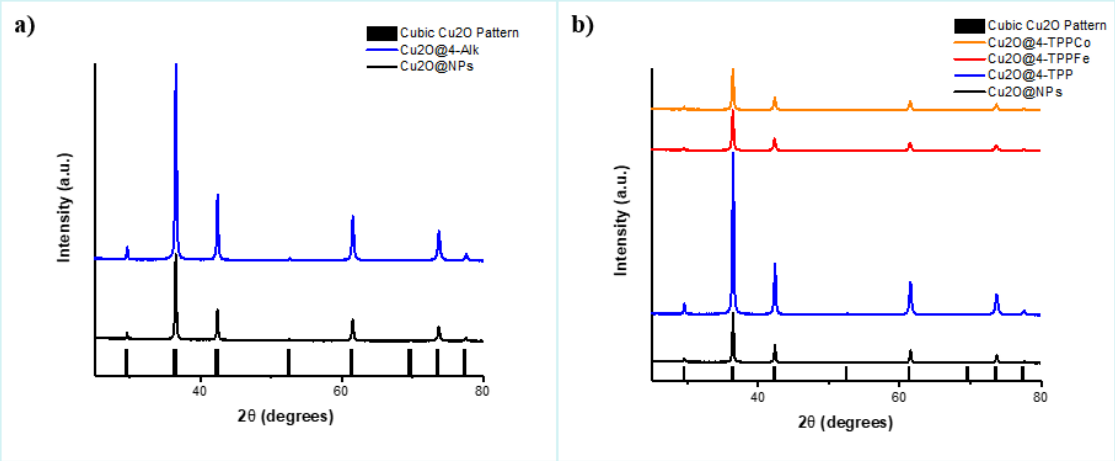

Figure 12. *PXRD spectra of a) Cu_2O@4-Alk and b) Cu_2O@4-TPP, Cu_2O@4-TPPCo, Cu_2O@4-TPPFe, both compared with Cu_2O@NCs.*

Powder X-Ray diffraction (PXRD) results of bare Cu_2O nanocubes showed peaks at 29.6, 36.4, 42.3, 61.4, 73.6 and 77.4º of 2θ values, which corresponds to (110), (111), (200), (220), (311), and (222) diffraction planes (Figure 12). This pattern closely matches with that characteristic of crystalline cubic Cu_2O.[30]

As shown by Figures 12a and 12b, the PXRD patterns of all the hybrid materials synthesized by using purely organic or metal-organic molecular building blocks showed the same diffraction peaks of bare Cu_2O NCs, indicating the structural retention of Cu_2O phase during the polymerization process of both hybrid materials. Moreover, no exogenous peaks are observed in the diffractogram, suggesting an amorphous character of the molecular polymer layer.

5.2. Attenuated Total Reflection – Infrared (ATR-FTIR)

The Attenuated total reflection technique is a sampling method that provides structural, vibrational, or chemical information about the sample of interest. With this technique, characteristic bands provide information about the type of material and layer that has been formed.

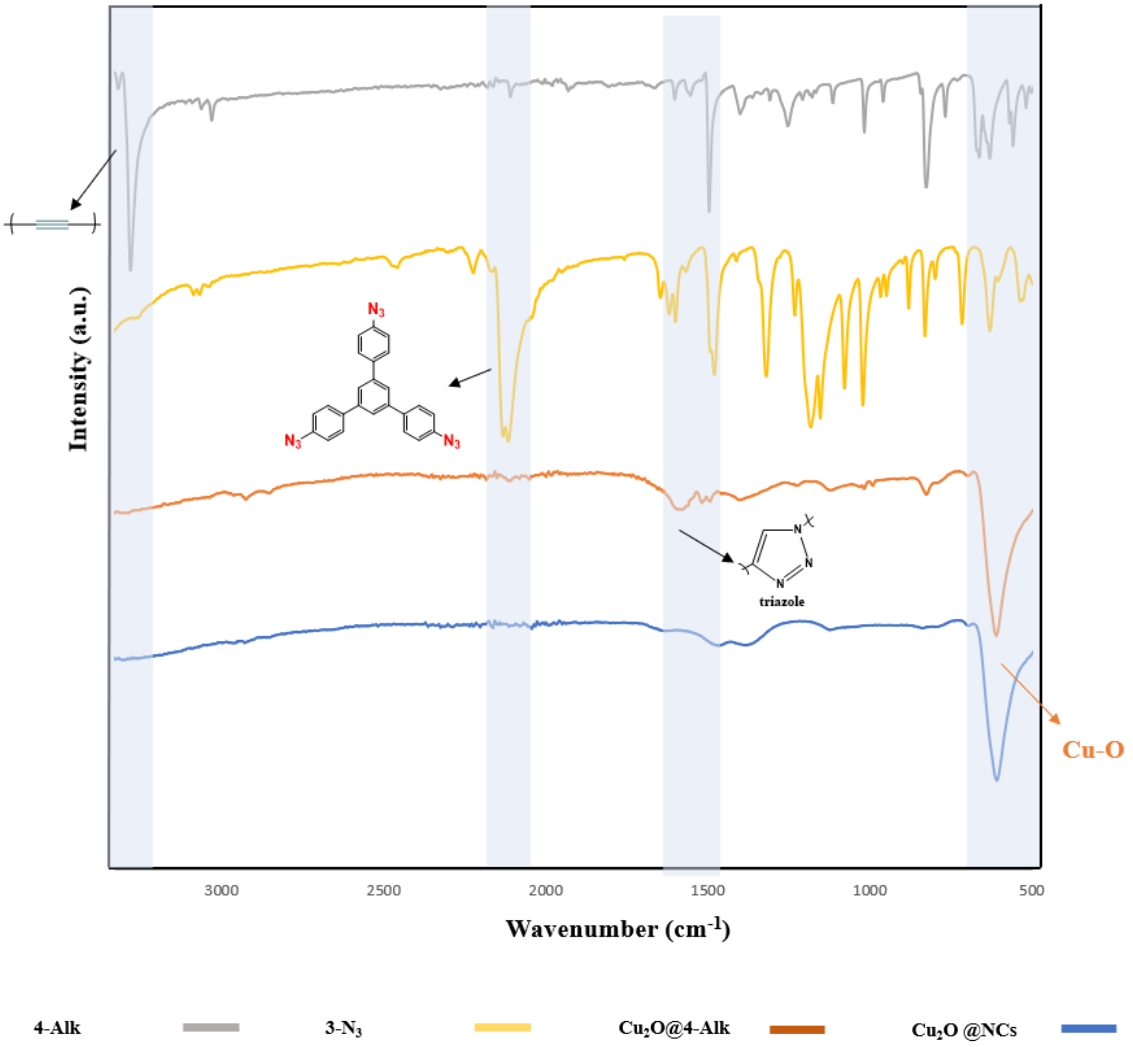

Figure 13. *ATR-FTIR spectrum of Cu_2O@4-Alk catalyst compared with Cu_2O@NCs and 3-N_3, 4-Alk monomers.*

The ATR infrared spectroscopy of Cu_2O@NCs and Cu_2O@4-Alk catalysts are represented in Figure 13, in blue and orange, respectively, and compared with 3-N_3 and 4-TPP monomers, in yellow and grey. For both catalysts, the spectra reveal the characteristic vibrational peak at 600 cm^{-1} which corresponds to the stretching vibration of Cu-O bond coming from pure Cu_2O,[34] indicating the retention of the copper oxide (I) structure during the polymerization process to obtain Cu_2O@4-Alk. Additionally, the

triazole is confirmed by the presence of the bands between 1400-1600 cm^{-1} coming from the 1,2,3-triazole moiety,[35] which reveals the successful formation of the metal-organic layer by click azide-alkyne cycloaddition reaction.

The 3-N_3 monomer spectra show the characteristic peak at 2100 cm^{-1}, which corresponds to the azide groups.[36] Moreover, the 4-Alk spectra show the characteristic peak at 3281 cm^{-1} arising from the presence of the terminal alkyne, which corresponds to the C-H stretching vibration.[35] The disappearance of these peaks in the hybrid material, and the appearance of the triazole peak points out that the monomers have reacted by click alkyne-azide polymerization reaction with no residual amount of monomers in the final material.

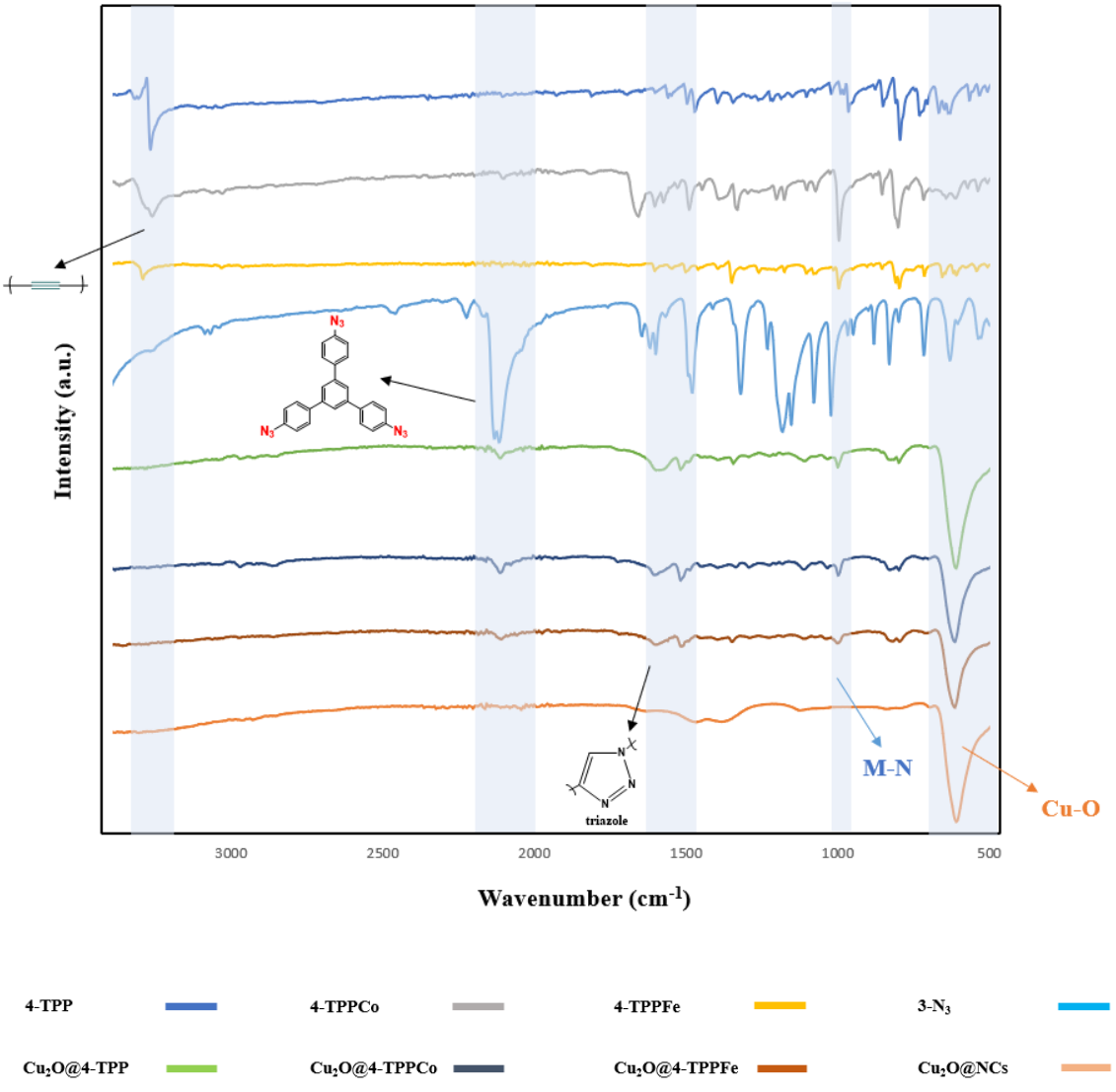

Figure 14. *ATR-FTIR spectra of Cu_2O@NCs, Cu_2O@4-TPP, Cu_2O@4-TPPCo and Cu_2O@4-TPPFe catalysts, compared with 4-TPP, 4-TPPCo, 4-TPPFe and 3-N3 monomers.*

The ATR infrared spectroscopy of the Cu_2O@NCs, Cu_2O@4-TPP, Cu_2O@4-TPPCo and Cu_2O@4-TPPFe catalysts, in orange, brown, blue, and green, are shown in Figure 14. As in the case of Cu_2O@4-Alk, all hybrid materials show the Cu-O stretching vibration at 600 cm^{-1} and the appearance of the triazole bands between 1400 cm^{-1} and 1600 cm^{-1} corresponding to 1,2,3-triazole moieties, revealing both, the structural retention of the cuprous oxide and the successful formation of the metal-organic layer surrounding the copper surface.

Focusing on the monomers, unlike the of Cu_2O@4-Alk catalyst analyzed in Figure 13, a small peak is observed at 2100 cm^{-1} corresponding to the azides groups. Even though the band has almost disappeared, a small peak still remains, coming hypothetically from the terminal unreacted azide groups from the end of the polymeric chain. That difference can be explained due to the different reactivity of the alkyne monomers. Since the 4-Alk monomer contains a quaternary carbon, the molecule has a 3D structure, thus facilitating the reaction with 3-N_3. On the other hand, the porphyrin monomers have a 2D structure, hindering the reaction with 3-N_3 on all four sides.

Finally, the spectrum of 4-TPP, 4-TPPCo and 4-TPPFe monomers, show the characteristic C-H stretching peak at 3200 cm^{-1} arising from the presence of the terminal alkyne, which is not seen in the hybrid catalyst spectra. Furthermore, the spectra of 4-TPPFe and 4-TPPCo also show the vibrational peak of Fe-N and Co-N at 1000 cm^{-1}, which are observed in the hybrid materials, supporting the successful incorporation of the Fe-porphyrin and Co-porphyrins moieties into the metal-organic layer.[30] In the case of Cu_2O@4-TPP the peak at 1000 cm^{-1} is also observed, suggesting that some Cu from cuprous oxide nanocubes may be coordinated to the metal-free porphyrins moieties as Cu(II) (see below).

The ATR spectroscopy results are consistent with the successful formation of the organic/metal-organic layer on each hybrid catalyst, demonstrating the high reproducibility and, robustness of the click alkyne-azide reaction, using different monomers with the same conditions.

5.3. Transmission Electron Microscopy (TEM)

The transmission electron microscopy (TEM) it is a technique used to analyze nanostructured materials and provides morphological information (particle size, and shape) and their distribution. With this technique, it is possible to probe the cubic shape and the nanoparticle size of the hybrid materials, as well as the morphological features of the organic/metal-organic layer.

- **Cu_2O nanocubes:**

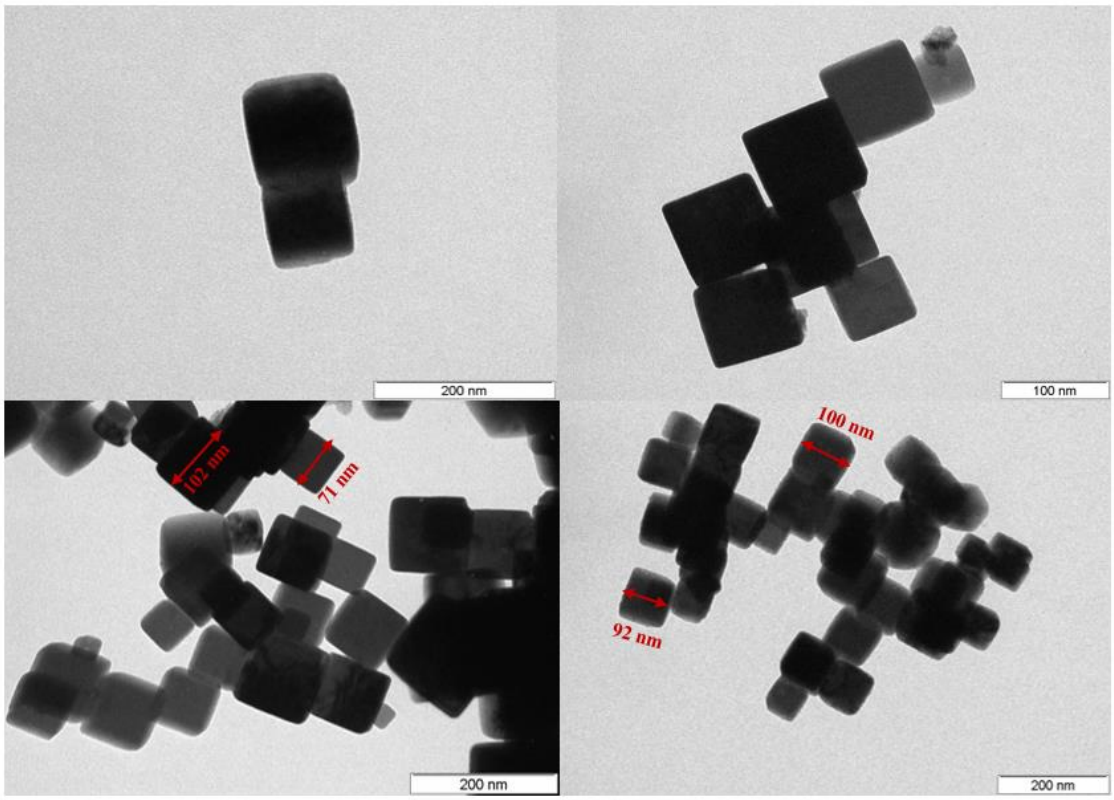

Figure 15. *TEM images of Cu_2O nanocubes.*

The transmission electron microscopy (TEM) images showed the cubic geometry of the Cu_2O nanocatalysts (Figure 15), confirming the cubic shape of the nanoparticles. The particles presented a size distribution between 80-100 nm, being reproducible in each batch synthesized. Despite no surfactants were used during the Cu_2O synthesis, the as-prepared Cu_2O nanocubes appear only slight aggregation.

- **Cu_2O@4-Alk**

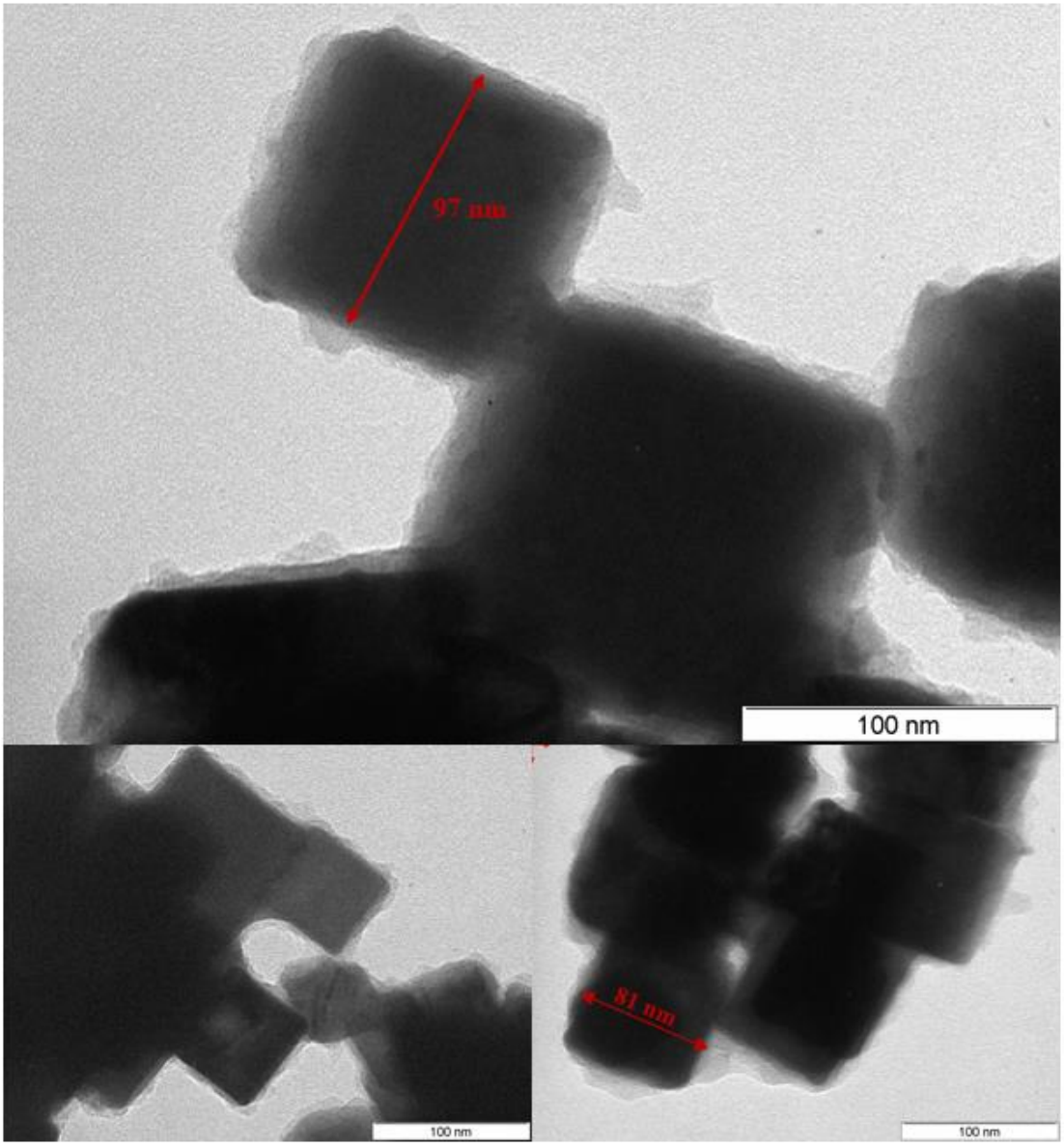

Figure 16. *TEM images of Cu_2O@4-Alk*

TEM images of Cu_2O@4-Alk are shown in Figure 16. The average size (distribution between 80-100 nm) and the cubic shape of the original particles is maintained during the click polymerization reaction, confirming the robustness of the Cu_2O NCs catalysts at the explored reaction conditions and a negligible Cu leaching during the reaction. Moreover, an irregular thin organic coating layer is apparent on the surface of the Cu_2O nanocubes, confirming the successful polymerization reaction occurring on the Cu_2O NCs surface. Compared to the other porphyrin-based alkynes used in this work, the 4-Alk monomer displays the unique capability of forming a 3D structure polymer around the Cu_2O NC

catalyst. According to the TEM images, the average thickness of the polymer layer wrapping around the particles is approximately 2 nm.

- **Cu_2O@4-TPP**

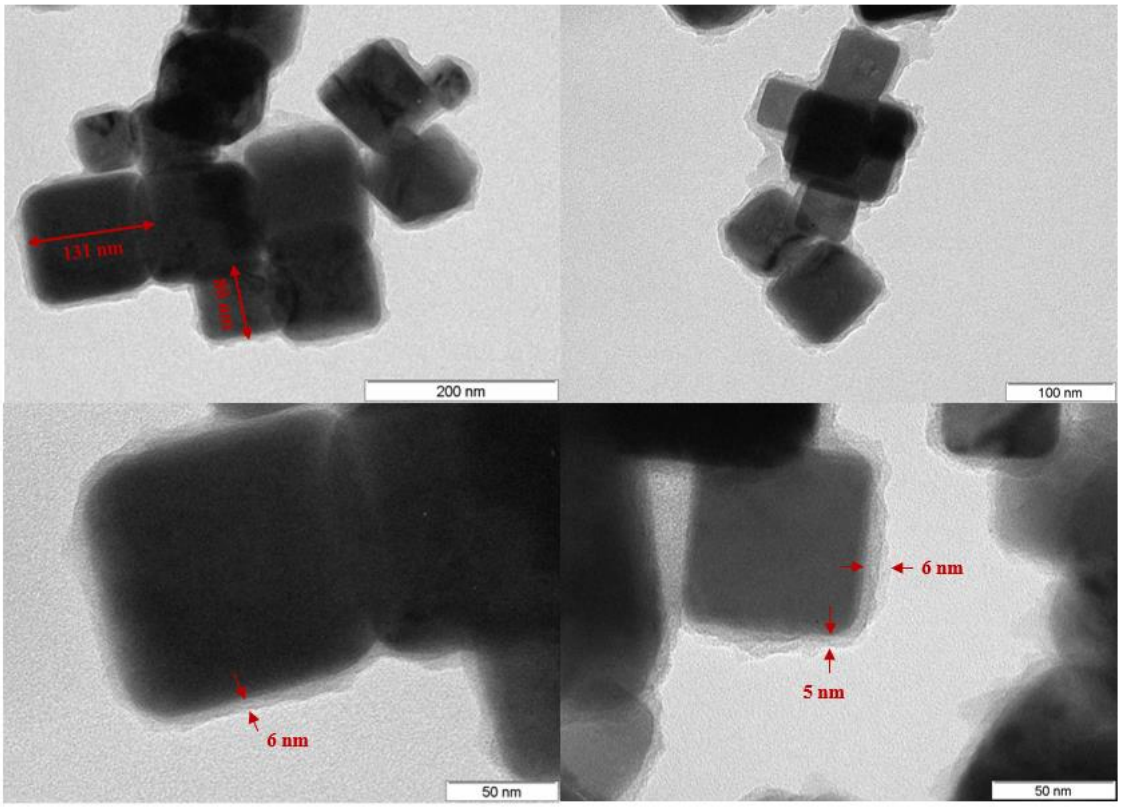

Figure 17. *TEM images of Cu_2O@4-TPP*

In Figure 17 are shown the TEM images of Cu_2O@4-TPP. Following the same trend than Cu_2O@4-Alk catalyst, the size and the shape of the nanoparticle are preserved after the polymerization reaction between 4-TPP and 3-N_3. The nanocubes distribution remains, presenting a small aggregation. Unlike the Cu_2O@4-Alk catalyst, the metal-organic layer formed is more uniform, presenting a thickness of 5-6 nm. On this occasion, the polymerization reaction occurred using the metal-free porphyrin (4-TPP). Since the 4-TPP monomer has a 2D structure and the fact that porphyrins can interact between them by π-π stacking, the formation of the metal-organic layer may be affected by stacking of polymeric chains on top of each other, resulting in an increased thickness of the coating observed in the images.

- **Cu_2O@4-TPPCo**

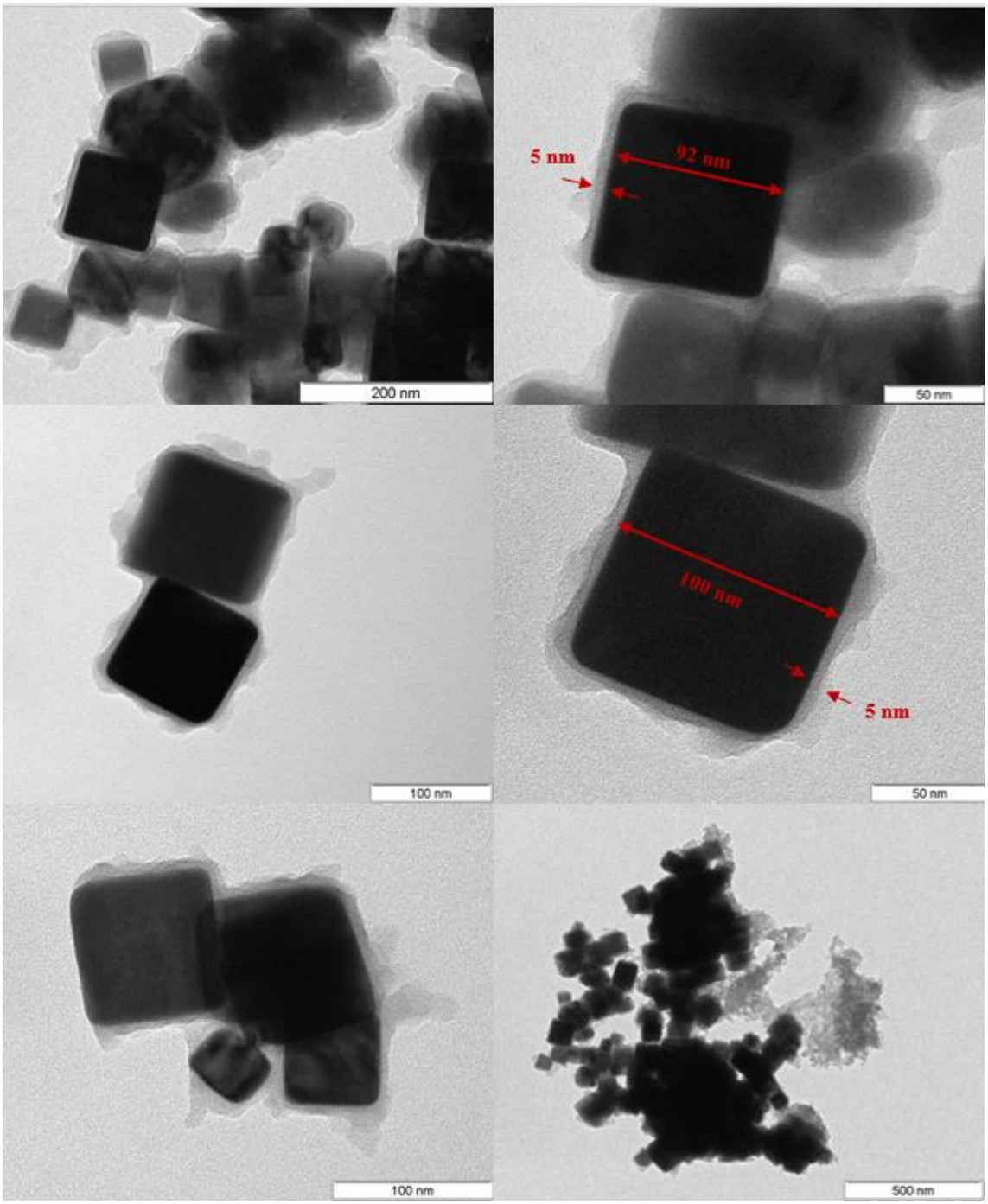

Figure 18. *TEM images of Cu_2O@4-TPPCo*

The TEM images of Cu_2O@4-TPPCo are shown in Figure 18. As previously mentioned for the organic hybrid materials, no changes have been observed in the shape or size of the nanoparticles. The metal-organic layer form has a thickness of 5-6 nm. Compared with the other hybrid materials mentioned, in some parts of the catalyst, the surrounding layer looks more irregular and less defined, suggesting some π-π stacking aggregation of

porphyrins. Furthermore, the lack of control on the π-π stacking interaction between the porphyrin units may also lead to an enhanced particle aggregation, as shown in Figure 18.

- **Cu_2O@4-TPPCo+**

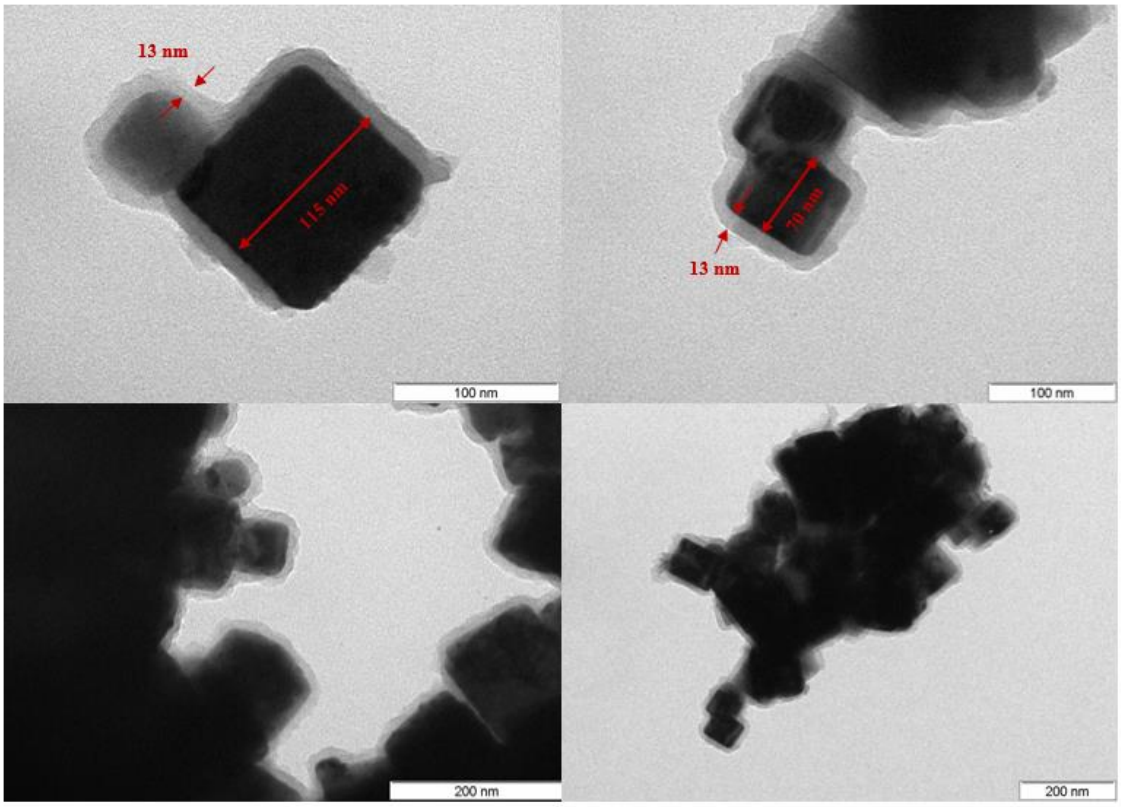

Figure 19. *TEM images of Cu_2O@4-TPPCo+*

In order to study the layer size control, the concentration of the monomers was doubled during the polymerization reaction, with the aim of forming a thicker layer. In the Figure 19, the TEM images of the Cu_2O@4-TPPCo+ are shown. Apart from the shape and size retention of the nanoparticles, the formation of a uniform layer can be observed, similar to Cu_2O@4-TPP catalyst. The thickness of the layer could be increased to 13 nm, pointing out that the layer can be modified and tuned by changing experimental parameters such as the concentration of the monomers. As discussed below, the effect of the coating thickness in catalysis was studied, with the aim to produce more CO to improve the C-C coupling step.

- **Cu_2O@4-TPPFe**

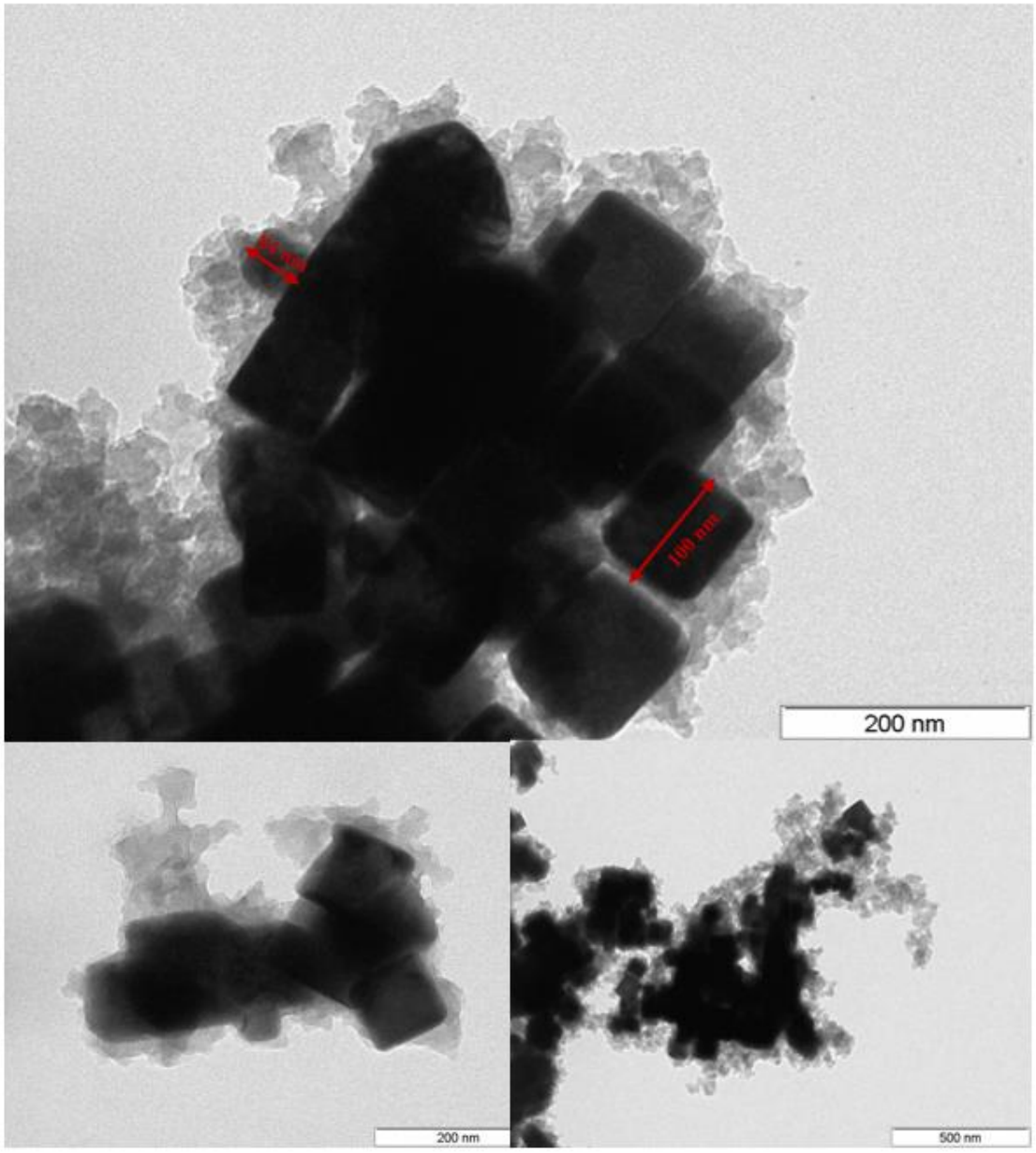

Figure 20. *TEM images of Cu_2O@4-TPPFe*

The TEM images of Cu_2O@4-TPPFe are shown in Figure 20. The shape and size of the particles are also maintained, following the trend of the other catalysts. It displays the formation of an amorphous matrix embedding the copper catalyst, forming aggregates of both, cuprous oxide nanocubes and 4-TPPFe monomer. Compared to the Cu_2O@4-TPPCo hybrid material, less control could be obtained in the formation of the metal-organic layer and stronger particle aggregation was observed, likely due to lower solubility of the 4-TPPFe monomer in the reaction mixture.

5.4. X-Ray Photoelectron Spectroscopy (XPS)

The X-Ray photoelectron spectroscopy (XPS) is able to obtain chemical composition of various material surfaces up to 1-2 nm depth. With this technique, it is possible to probe out the surface composition of a material and the oxidation state of its elements.

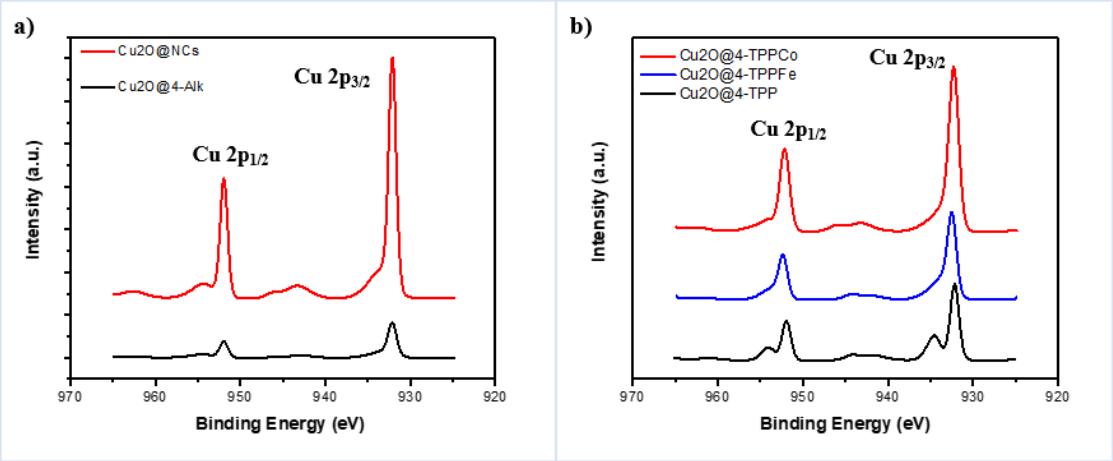

Figure 21. *XPS spectra of a) Cu_2O@NCs, Cu2O@4-Alk and b) Cu_2O@4-TPP, Cu_2O@4-TPPFe, Cu_2O@4-TPPCo*

X-ray photoelectron spectroscopy (XPS) of Cu_2O@NCs and Cu_2O@4-Alk, in red, and black, respectively, are shown in Figure 21a. The spectra of each catalyst reveal the Cu $2p_{1/2}$ and $2p_{3/2}$ orbital peaks at 950.9 and 930.9 eV respectively,[30] indicating that Cu (I) is the unique oxidation state in both hybrid catalysts, confirming the stability of Cu_2O nanoparticles after their use as a catalyst in the click reaction.

The Figure 21b shows the XPS of Cu_2O@4-TPP, Cu_2O@4-TPPFe, and Cu_2O@4-TPPCo, in black, blue, and red, respectively. The spectra of each catalyst also reveal the Cu $2p_{1/2}$ and $2p_{3/2}$ orbital peaks at 950.9 and 930.9 eV, confirming the presence of Cu(I) as a dominant oxidation state in the catalysts. Nevertheless, in the case of Cu_2O@4-TPP, two other orbital peaks are observed at 954.1 and 934.1 eV, which correspond to Cu(II).[37] The presence of Cu(II) in the spectra suggest that partial etching of copper from Cu_2O NCs occurred during the reaction, followed by oxidation to Cu(II) and coordination within the porphyrin ring, thus forming Cu(II)-porphyrins moieties in the metal-organic layer.

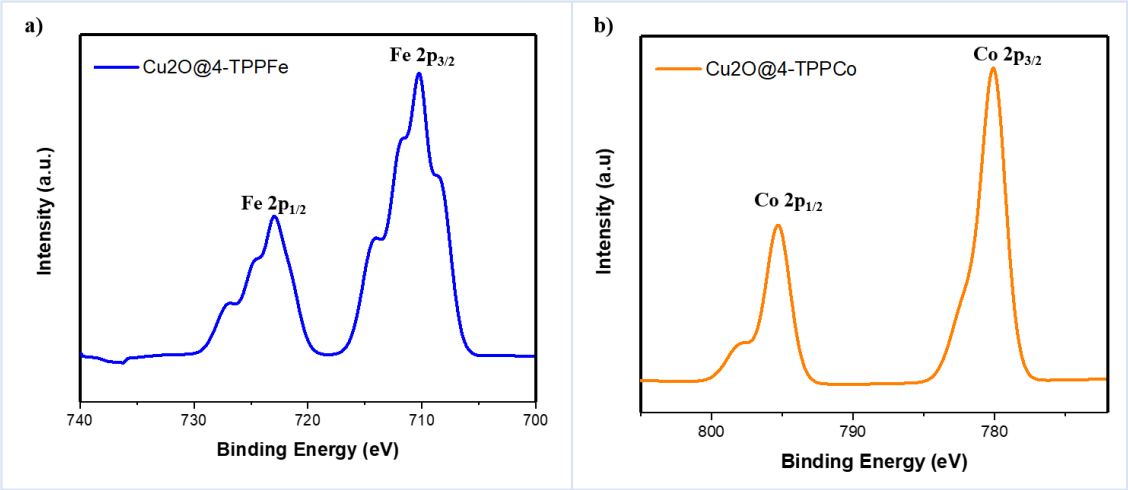

Figure 22. *XPS spectra of a) Cu_2O@4-TPPFe and b) Cu_2O@4-TPPCo*

The XPS spectra of Cu2O@4-TPPFe, in blue, is shown in Figure 22a. The peak of lower binding energy, at 709.62 eV, is assigned to the Fe $2p_{1/2}$ orbital peak, while the peak of higher binding energy, at 722.78 eV, is assigned to the Fe $2p_{3/2}$ orbital peak. These features are in excellent agreement with XPS data reported for materials based on Fe(III) porphyrins, thus confirming the presence of Fe-porphyrin moieties in the surface layer wrapping around the Cu_2O NCs in the hybrid materials.[38]

In a similar fashion, the XPS spectra of Cu2O@4-TPPCo (Figure 22b) display a peak at 780.6 eV corresponding to the Co $2p_{1/2}$ peak, while the peak at higher binding energy (796.1 eV), corresponds to the Co $2p_{3/2}$ orbital peak. These features are consistent with the incorporation of Co(II)-porphyrin units in the metal-organic layer covering the Cu_2O core of Cu_2O@4-TPPCo.[10]

5.5. Electrocatalysis

5.5.1. Model molecular macrocyclic systems

Before testing the cuprous oxide nanocubes and the hybrid materials, two well-known molecular catalysts have been tested in order to check the equipment employed for the catalysis experiments.

First of all, a cobalt (II) phthalocyanine (CoPc) was immobilized onto carbon nanotubes (CoPc/MWCNTs) and used to test the electrochemical and the detection systems. Moreover, a cobalt (II) tetraphenylporphyrin (CoTPP) was immobilized onto carbon nanotubes (CoTPP/MWCNTs) and used as a reference system since it was one of the monomers employed during the synthesis of the hybrid materials.

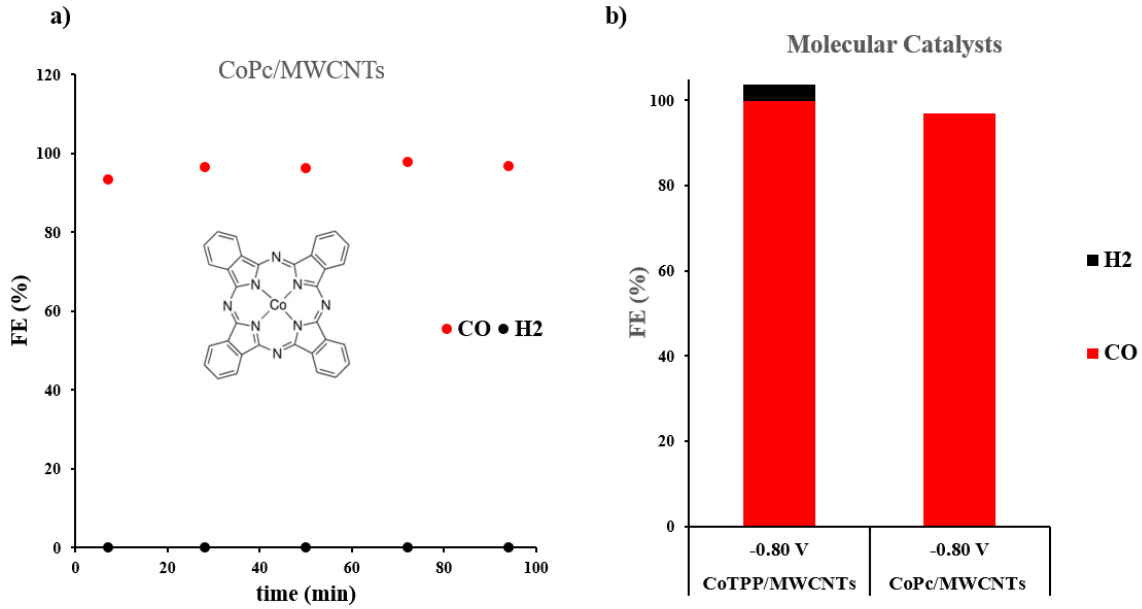

Figure 23. *Faradic products efficiencies (FEs) obtained using a) CoPc/MWCNTs and b) CoTPP/MWCNTs compared with CoPc/MWCNTs, at -0.8V vs RHE*

In Figure 23 are shown the CO and H_2 FE for both molecular catalysts after the electrolysis performance at -0.8 V vs RHE. The CoPc/MWCNTs showed an excellent selectivity towards the formation of CO with a FE of 97% (Figure 23a), in agreement with the results reported from previous literature. A sustained selective catalytic CO_2-to-CO conversion was observed during electrolysis, without any detected amount of hydrogen.

Analogous results were obtained for CoTPP/MWCNTs, which presented a nearly quantitative formation of CO (FE = 99%) under the same conditions, with only very minor

traces of H_2 (3%) (Figure 23b). These data confirm the effectiveness of the CoTPP molecular unit to catalyze CO_2RR to CO, in line with previous reports.

5.5.2. Cu_2O Nanocubes

The cuprous oxide nanocubes were tested at different potential in order to obtain a general overview of selectivity variation from C_1 to C_2 products as function of the applied overpotential (Figure 24).

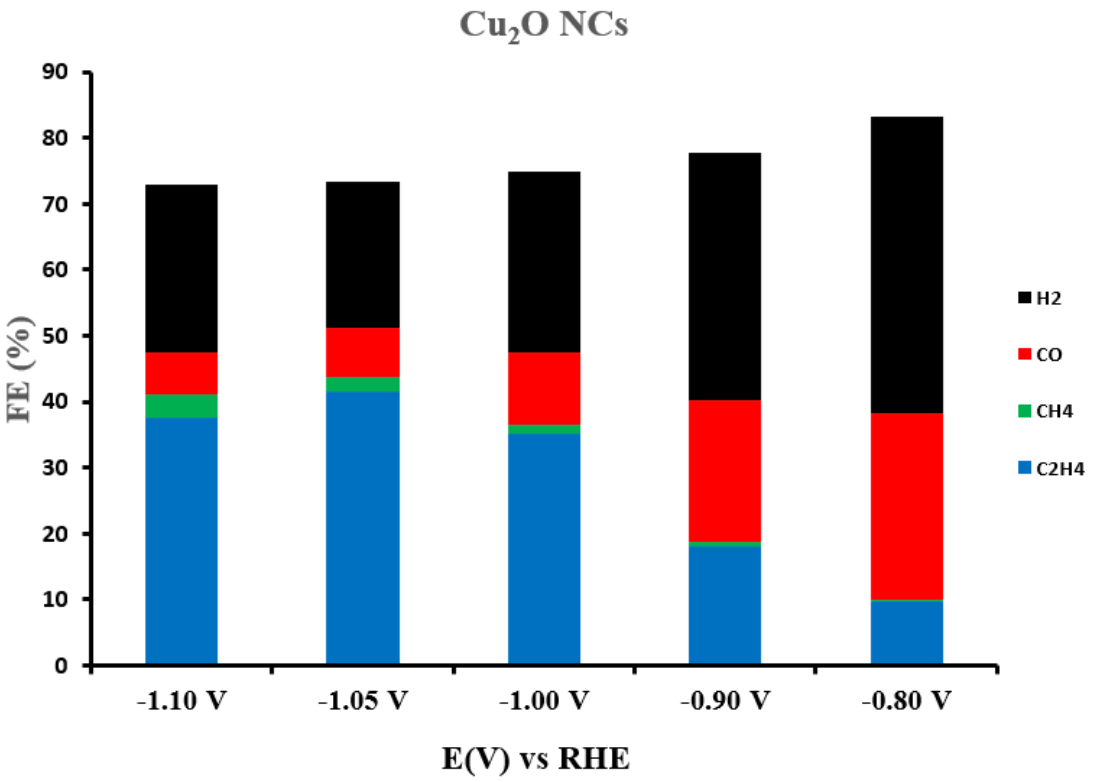

Figure 24. *Faradic products efficiencies (FEs) obtained from the CO_2 electroreduction as a function of the applied electrode potential after 100 minutes of reaction time, using Cu_2O nanocubes.*

The results obtained from the electrolysis experiments of the Cu_2O nanocubes at different potentials show a clear trend in which the selectivity to CO and H_2 is favored at low overpotentials while the selectivity progressively shifts towards C_2H_4 production upon increasing overpotentials. For applied potentials below -1.0 V vs RHE CH_4 production starts to occur and the efficiency of the CO_2-to-CH_4 process tends to increase by increasing overpotentials (Figure 24). This trend can be visualized in Figure 25. At low overpotential, the two-electron CO_2 reduction pathway to CO is the main CO_2RR process taking place on the copper surface, leading to release of CO as dominant product. By

increasing the overpotential, the local CO concentration increases at the copper surface, thus favoring the C-C coupling step between two *CO, producing C_2H_4 as dominant product and decreasing the FE of CO. Finally, when a high overpotential is applied, the further multi-electron reduction of the adsorbed *CO favorably competes with the chemical steps, leading to progressively diminished FE for C_2H_4 and CO production, respectively, upon increasing overpotential.

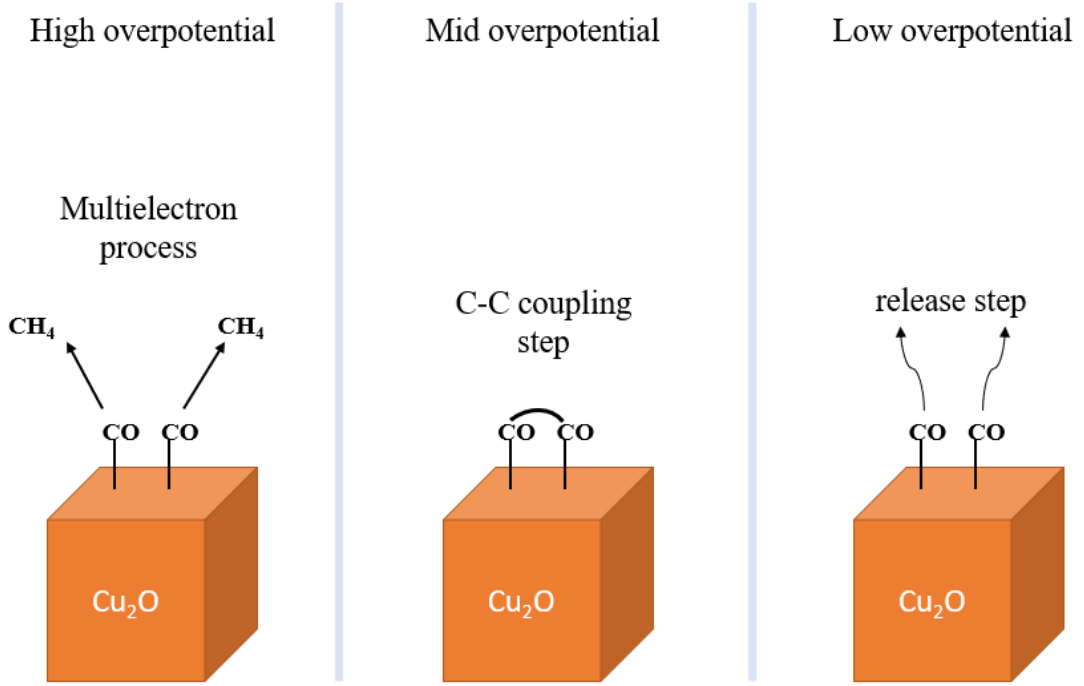

Figure 25. *Proposed simplified CO_2RR pathways scheme to explain the variation in selectivity of Cu_2O NCs as function of the applied potential.*

At -0.8 V vs RHE, CO and H_2 were found to be the major products in the gas phase, with a maximum FE for CO of around 28%. At this applied potential, C_2H_4 production starts to occur even though with low efficiencies (9,73%). The highest FE for C_2H_4 was obtained at -1.05 V vs RHE, corresponding to 42%, with a simultaneous decrease of FE for CO and H_2. When a higher potential was applied, the FE of C_2H_4 was slightly reduced, and methane production increased up to a FE of 3% at -1.10 V vs RHE. These results are consistent with the CO_2RR performances reported in similar conditions for smaller Cu_2O nanocubes.[39] Roldan, Strasser et al. reported an analogous selectivity trend for 30-35 nm sized Cu_2O nanocube catalysts, showing a maximum faradaic efficiency of 34% for C_2H_4 at -0.97 V vs RHE, and predominant CO production at low overpotentials.[39]

5.5.3. Cu_2O-based hybrid materials

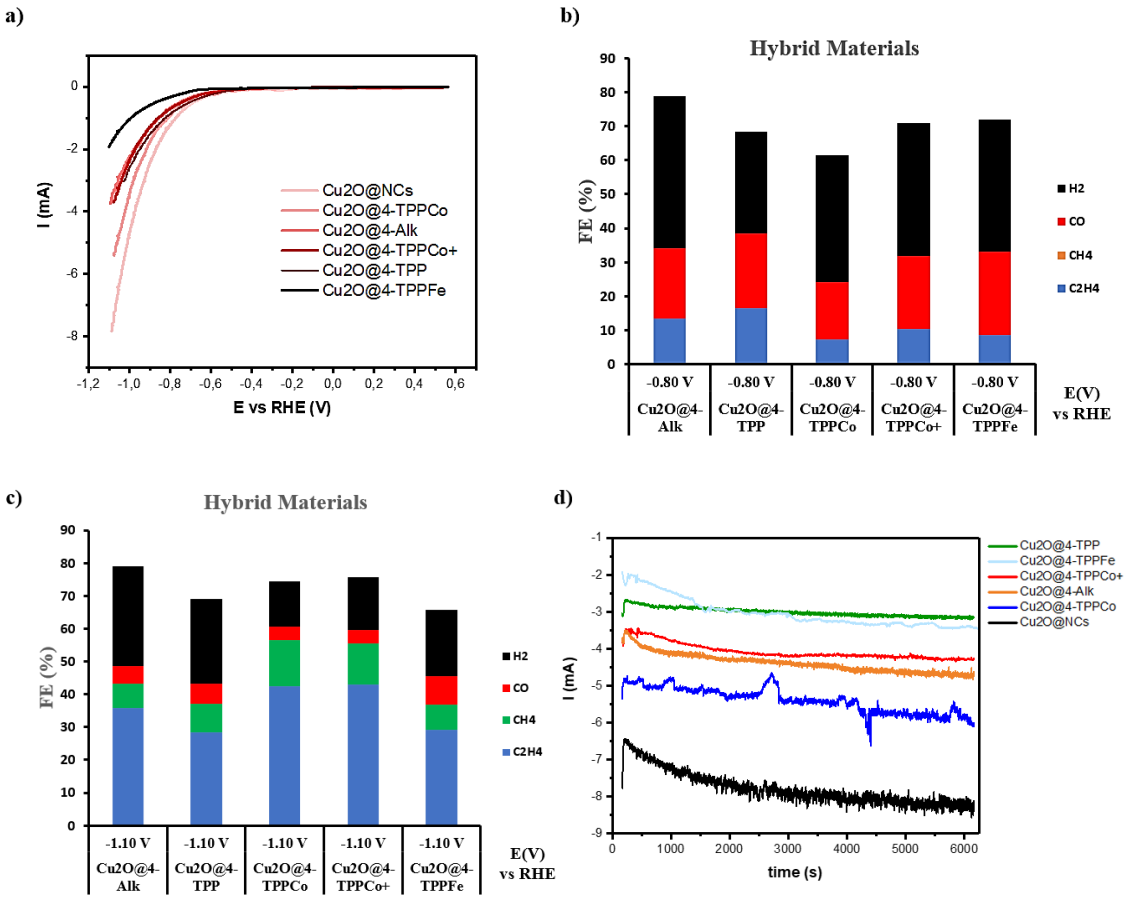

Figure 26. *a) LSVs of all hybrid materials compared with Cu_2O NCs. Selectivity data for the CO_2 electroreduction catalyzed by all the hybrid materials studied herein at -0.80V vs RHE (b) and at -1.10V vs RHE (c) after 100 minutes of electrolysis. d) Chronoamperometric experiments of all hybrid materials at -1.10V vs RHE compared with bare Cu_2O NCs.*

As shown in Figure 26a, the polymer-free Cu_2O NCs displayed a higher current density compared to the hybrid materials, likely due to partial saturation of the Cu-based active sites by polymer coverage in the latter. In this regard, the organic/metalorganic polymer coating probably possesses low conductivity, thus limiting the overall current density available for CO_2RR. Linear scan voltammograms also indicate that the onset potential for CO_2RR is at around -0.6 V vs RHE for all the catalysts, except for Cu_2O@4-TPPFe which was found to occur at slightly more negative potentials (-0.67V vs RHE) (Figure 26a).

Chronoamperometric experiments under CO_2-saturated conditions were carried out at -0.80 V and -1.10 V vs RHE, respectively, to compare the activity and selectivity of the Cu_2O-based hybrid materials and the bare Cu_2O NCs. In general, the hybrid catalysts were found to display an analogous CO_2RR selectivity trend previously discussed for the polymer-free Cu_2O NCs. When a low overpotential was applied (Figure 26b), the results did not show significant differences compared to bare Cu_2O NCs. The predominant products formed were H_2 and CO with FEs around 30-44% and 17-24%, respectively. C_2H_4 was detected as a minor product (FE = 7-12%), while no CH_4 was detected during the experiments. As expected, higher overpotentials tend to enhance the efficiency towards the formation of multi-electron products like C_2H_4 and CH_4 (Figure 26c). At -1.10 V vs RHE, Cu_2O@4-TPPCo was found to produce C_2H_4 (42%) and CH_4 (14%) with the highest FEs in the series of the tested hybrid catalysts. Although the FE for C_2H_4 formation is comparable to that obtained by bare Cu_2O NCs under the same conditions, Cu_2O@4-TPPCo showed a 4.16-fold increase of FE toward CH_4 production as well as a considerably lower HER (FE = 14%). Conversely, the Cu_2O@4-Alk, characterized by a purely organic polymer wrapping around the NCs, showed a slightly decreased selectivity to C_2H_4 (FE = 35%) and a significantly higher efficiency for H_2 evolution (31%) compared to bare Cu_2O NCs (FE = 25%). Moreover, strikingly similar selectivity data were obtained for Cu_2O@4-TPPCo and Cu_2O@4-TPPCo+, indicating that the product distribution is relatively insensitive to the thickness of the porphyrin-based polymeric layer. Taken together, these results suggest that the nanostructured Cu component is the main responsible for the CO_2 electroreduction catalyzed by the hybrid materials and the observed selectivity changes compared to the bare Cu_2O NCs are likely due to the specific potential-dependent morphological evolution of the Cu catalyst influenced by the polymeric matrix rather than coming from a direct involvement of the polymer in the catalytic CO_2RR reaction. Notably, during the chronoamperometric tests at -1.10 V vs RHE, the current remained stable for all catalysts, showing the good stability of the catalysts over 100 minutes of electrolysis (Figure 26d).

Across the series, Cu_2O@4-TPPFe displayed the lowest catalytic current density under CO_2 atmosphere (Figures 26a,d). This may be related to the stronger particle aggregation occurring during in the in-situ polymerization click reaction, as evidenced by TEM images (see above). An extensive study of the Cu_2O@4-TPPFe catalyst was performed

in order to understand the metalorganic polymer effect in selectivity and catalysis as a function of the applied potential. (Figure 27).

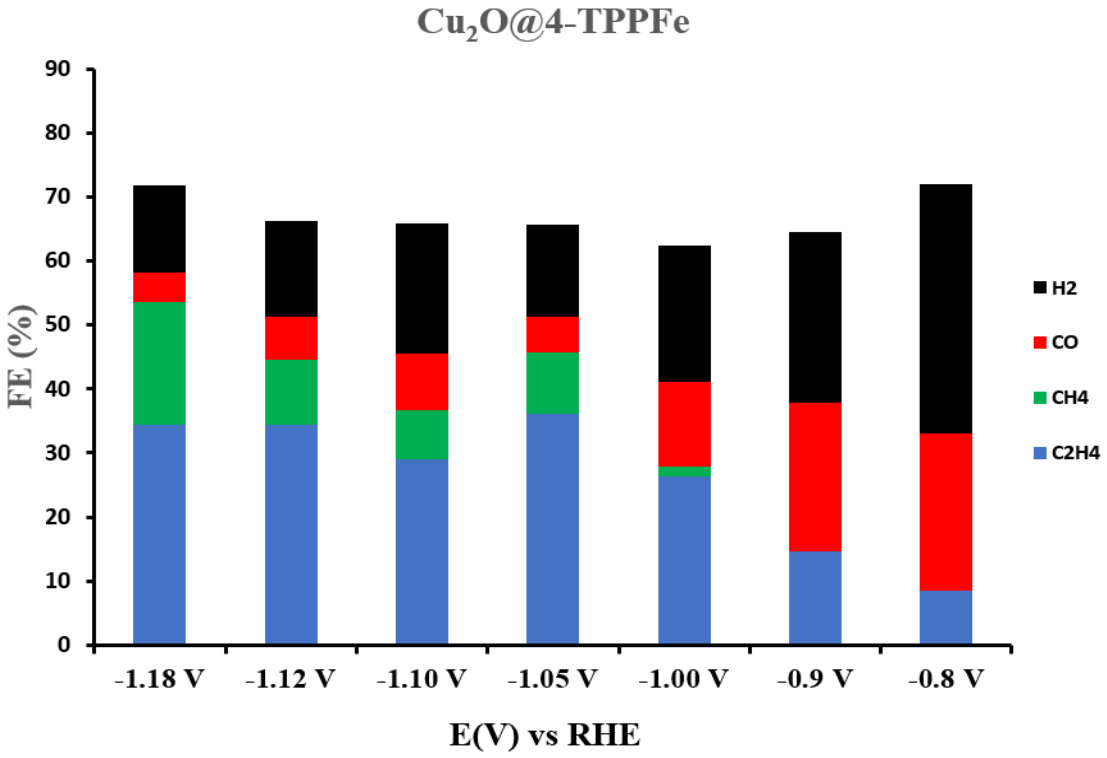

Figure 27. *FE obtained from the CO_2 electroreduction as a function of the applied potential (vs RHE) after 100 minutes of electrolysis, using Cu_2O@4-TPPFe hybrid material.*

The potential-dependent selectivity data of Cu_2O@4-TPPFe provided analogous results to those previously discussed for the polymer-free Cu_2O NCs (Figure 24). However, the presence of the Fe porphyrin polymer leads to a slight increase of the FE for CH_4 production, obtaining a 10% FE at -1.05 V vs RHE versus 2% FE obtained with the bare Cu_2O NCs. As expected, the selectivity towards CH_4 increases at more negative potentials, resulting in a maximum FE = 19% at -1.18 V vs RHE. As previously mentioned, the enhanced efficiency for CH_4 formation observed for the porphyrin-based hybrid Cu_2O NCs may be mostly due to some morphological and size changes of the particles under electrochemical conditions, which may lead to isolated amorphous copper particles encapsulated by polymeric matrices. In this regard, Roldan et al. recently reported some evidence of the particle size effect in CO_2RR selectivity for Cu nanoparticles. When particles around 35 nm were employed, an exponential increment of faradic selectivity towards CH_4 was reported.[40] Furthermore, concomitantly to the CH_4 increment, the FE of H_2 was slightly reduced. At low overpotentials, as it was expected, there were no differences, where the H_2 and CO were the dominant products.

6. CONCLUSIONS

This study presents an innovative method for the rational design of hybrid heterogeneous-molecular Cu-based nanomaterials for CO_2RR, using well-defined Cu_2O nanocubes as reference system. The Cu_2O NCs were first successfully synthesized and characterized by using spectroscopic and microscopic techniques. Furthermore, they were successfully employed as both templates and catalysts for an in-situ polymerization reaction based on azide-alkyne ‘’click’’ reaction between molecular building blocks. The resulting hybrid nanomaterials were also characterized by using spectroscopic and microscopic techniques, showing evidence of the formation of organic or metal-organic polymer layer coating. The structural integrity of the original Cu_2O nanocubes was maintained during the polymerization reaction, without any evidence for significative copper leaching nor the formation of new crystalline phases during the reaction. The hybrid materials displayed an average thickness of a few nanometers for the amorphous polymer layer wrapping around the cubic particles, which was modified by tuning the reaction conditions (e.g. the monomer concentration) or the type of linkers. For hybrid nanocatalysts based on click metalloporphyrin polymers, strong π-π stacking interaction between the porphyrin moieties and limited solubility of the molecular precursor were found to induce strong particle aggregation during the polymerization reaction.

The catalytic performances of hybrid nanomaterials were tested in a H-type electrochemical cell setup with an online gas-chromatographic quantification analysis and found to be competent electrocatalysts for CO_2RR, obtaining a mixture of C_1-C_2 gaseous products (primarily CO, C_2H_4, CH_4 in addition to H_2) in neutral pH electrolyte. The bare Cu_2O NCs showed a potential-dependent selectivity consistent with previous literature, where CO and H_2 production is favored at low overpotential while the selectivity towards C_2H_4 and CH_4 increases at higher overpotentials, with a maximum FE = 42% for C_2H_4 formation at -1.05 V vs RHE. The hybrid catalysts displayed an analogous selectivity trend. A slight preference for HER was obtained in the case of Cu_2O@4-Alk, based on a purely organic polymer. The metalloporphyrin-based hybrid materials provided similar FEs for C_2H_4 production compared to bare Cu_2O NCs, but also a slightly improved selectivity towards CH_4 formation. The minor selectivity changes observed for the hybrid nanomaterials compared to the original Cu_2O NCs are likely ascribed mainly to nanostructured copper catalyst, whereas the polymeric matrix is supposed to play a role in influencing the potential-dependent morphological evolution

of the Cu catalyst, rather than participating directly in the catalytic CO_2RR process. In general, the efficiency of the hybrid catalysts is hindered by the poorly conductive character of the amorphous polymer coverage and by the aggregation phenomena occurring during the in situ polymerization click reaction, which strongly limit their CO_2RR performances and reduce the number of active sites on the surface.

Taking these aspects into consideration, possible points for future improvement of these hybrid Cu-based nanocatalysts include the use of smaller nanocubes as catalysts or the use of surfactants for the synthesis of the nanocubes, in order to favor an homogeneous dispersion of the particles. Moreover, tuning the reaction conditions (e.g. diluted monomer concentration) and/or the nature of the molecular building blocks could be used to minimize the particle aggregation effects and optimize the polymer layer. Additionally, the current densities for the hybrid materials could be improved by dispersing Vulcan or MWCNTs with the catalyst ink. Finally, in a more applicative perspective, other substrates, such as copper foil or foam, could be used instead of well-defined Cu_2O nanoparticles as templates and catalysts for the polymerization reaction.

Current efforts are also focused on improving the characterization of the hybrid nanomaterials before and after electrocatalysis in order to obtain further information about the spatial conformation of organic/metalorganic layer formed around the Cu core and about the dynamic evolution of the catalyst morphology and oxidation state during the CO_2RR. We are also currently focused on completing the analysis and quantification of the liquid products formed during CO_2 electroreduction, which will be provided by a combination of ^{1}H-NMR analysis and ion chromatography. Preliminary analysis provided evidence of formation of ethanol, propanol, acetate, and formate as major species in the liquid phase.

7. ACKNOWLEDGEMENTS

This work and research behind would not have been possible without the exceptional support from ICIQ, which granted me a master's scholarship for full time studies in order to achieve the master's degree. I am especially indebted to my supervisor, Prof. Emilio Palomares, who kindly received me into his exceptional research group. His knowledge, experience and exacting attention to detail have been an inspiration and have helped me to carry out this thesis.

I am grateful to all of the members of Palomares's group, whom I have had the pleasure to work during this project. With them, I have been able to expand my knowledge about both, scientific research, and life in general, providing me an extensive personal and professional guidance. I would especially like to thank Dr. Federico Franco, who together with Prof. Emilio, have become a scientific role model. As my teacher and mentor, he has taught me, in a first-hand experience, scientific knowledge for which I am eternally grateful, and, how to become a great researcher. I would also like to thank Dra. Eugenia Martínez, for her advice and assistance in keeping my progress on schedule. I would also want to thank the technicians from ''research support units'', for their assistance in providing me with the resources I needed to develop the project.

I would like to show gratitude to the master's coordination, Prof. Antonio M. Echavarren and Prof. Jose Manuel Ricard Pla, and all the professors from ''Synthesis, Catalysis and Molecular design'' URV-ICIQ master, who have been supportive of my career goals and who worked actively giving unique lectures.

I would also like to extend my gratitude to the technicians of the following organizations for helping me to obtain data not available at ICIQ:

- Dr. Sergi Plana and Dra. Rita Marimon, from Servei de Recursos Científics i Tècnics (SRCiT), Universitat Rovira i Virgili.
- Dr. Fernando Coloma, from X-Ray unit, Universidad de Alicante.

Finally, nobody has been more important to me in the pursuit of this project than the members of my family and my friends. I would especially like to thank my parents; whose love and guidance are with me in whatever since I was born. They are the ultimate role models.

8. BIBLIOGRAPHY

[1] Duan, X.; Xu, J.; Wei, Z.; Ma, J.; Guo, S.; Wang, S.; Liu, H.; Dou, S. Metal-Free Carbon Materials for CO_2 Electrochemical Reduction. *Adv. Mater.*, **2017**, *29* (41), 1–20.

[2] Franco, F.; Rettenmaier, C.; Jeon, H. S.; Cuenya, B. Transition metal-based electrochemical CO_2 reduction: from atoms and molecules to nanostructured materials. *Chem. Soc. Adv.*, **2020**, *49*, 6884.

[3] Gattrell, M.; Gupta, N. A review of the aqueous electrochemical reduction of CO_2 to hydrocarbons at copper. *Journal of Electro. Chem.*, **2006**, *594*, 1-19.

[4] Tan, X. T.; Sun, X.; Han, B.; Ionic liquid-based electrolytes for CO_2 electroreduction and CO_2 electroorganic transformation. *Nat. Sci. Rev.*, **2022**, *9*, 1-18.

[5] Francke, R.; Schille, B.; Roemelt, M. Homogeneously Catalyzed Electroreduction of Carbon Dioxide—Methods, Mechanisms, and Catalysts. *Chem. Rev.*, **2018**, *9*, 4631-4701.

[6] Boutin, E.; Merakeb, L.; Ma, B.; Boudy, B.; Wang, M.; Bonin, J.; Anxolabéhère-Mallart, E.; Robert, M. Molecular catalysis of CO_2 reduction: recent advances and perspectives in electrochemical and light-driven processes with selected Fe, Ni and Co aza macrocyclic and polypyridine complexes. *Chem. Soc. Rev.*, **2020**, *16*, 5772.

[7] Nicklas W.; Werlé, C.; Leitner, W. Transition Metal Complexes as Catalysts for the Electroconversion of CO_2: An Organometallic Perspective. *Angew. Chem. Int. Ed.*, **2021**, *60*, 11628-11686.

[8] Weng, Z.; Jiang, J.; Wu, Y.; Wu, Z.; Guo, X.; Materna, K. L.; Liu, W.; Batista, V. S.; Brudvig, G. W.; Wang, H. Electrochemical CO_2 Reduction to Hydrocarbons on a Heterogeneous Molecular Cu Catalyst in Aqueous Solution. *J. Am. Chem. Soc.*, **2016**, *138* (26), 8076-8079.

[9] Feng, S.; Zheng, W.; Zhu, J.; Li, Z.; Yang, B.; Wen, Z.; Lu, J.; Lei, L.; Wang, S.; Hou, Y. Porous metal-porphyrin triazine-based frameworks for efficient CO_2 electroreduction. *Applied Catalysis B: Environmental.*, **2020**, *270*, 118908.

[10] Hu, X. M.; Ronne, M. H.; Pedersen, S. U.; Skydstrup, T.; Daasbjerg, K. Enhanced Catalytic Activity of Cobalt Porphyrin in CO_2 Electroreduction upon Immobilization on Carbon Materials. *Angew. Chem. In. Ed.*, **2017**, *56* (23), 6468-6472.

[11] Azcarate, I.; Costentin, C.; Robert, M.; Savéant, S. Through-Space Charge Interaction Substituent Effects in Molecular Catalysis Leading to the Design of the Most Efficient Catalyst of CO_2-to-CO Electrochemical Conversion. *J. Am. Chem. Soc.*, **2016**, *138* (51), 16639-16644.

[12] Costentin, C.; Drouet, S.; Passard, G.; Robert, M.; Savéant, J. M. Proton-Coupled Electron Transfer Cleavage of Heavy-Atom Bonds in Electrocatalytic Processes. Cleavage of a C–O Bond in the Catalyzed Electrochemical Reduction of CO_2. *J. Am. Chem. Soc.*, **2013**, *135* (24), 9023-9031.

[13] Costentin, C.; Passard, G.; Robert, M.; Savéant, J. M. Pendant Acid–Base Groups in Molecular Catalysts: H-Bond Promoters or Proton Relays? Mechanisms of the Conversion of CO_2 to CO by Electrogenerated Iron(0)Porphyrins Bearing Prepositioned Phenol Functionalities. *J. Am. Chem. Soc.*, **2014**, *136* (33), 11821-11829.

[14] Costentin, C.; Robert, M.; Savéant, J. M. Current Issues in Molecular Catalysis Illustrated by Iron Porphyrins as Catalysts of the CO_2-to-CO Electrochemical Conversion. *Acc. Chem. Res.*, **2015**, *48* (12), 2996-3006.

[15] Torbensen, K.; Han, C.; Boudy, B.; Von Wolff, N.; Bertail, C.; Braun, W. Robert, M. Iron Porphyrin Allows Fast and Selective Electrocatalytic Conversion of CO_2 to CO in a Flow Cell. *Chem. Eur. J.*, **2020**, *26* (14), 3031-3038.

[16] Torbensen, K.; Han, C.; Boudy, B.; Von Wolff, N.; Bertail, C.; Braun, W. Robert, M. Iron Porphyrin Allows Fast and Selective Electrocatalytic Conversion of CO_2 to CO in a Flow Cell. *Chem. Eur. J.*, **2020**, *26* (14), 3031-3038.

[17] Ren, S.; Joulié, D.; Salvatore, D.; Torbensen, K.; Berlinguette, C. P. Molecular electrocatalysts can mediate fast, selective CO_2 reduction in a flow cell. *Science.* **2019**, *365* (6451), 367-369.

[18] Gao, D.; Zhang, Y.; Zhou, Z.; Cai, F.; Zhao, X.; Huang, Z.; Li, Y.; Zhu, J.; Liu, P.; Yang, F.; Wang, G.; Bao, X. Enhancing CO2 Electroreduction with the Metal−Oxide Interface. *J. Am. Chem. Soc*, **2017**, *139* (16), 5652-5655.

[19] Franco, F.; Rettenmaier, C.; Jeon, H. S.; Cuenya, B. Transition metal-based electrochemical CO_2 reduction: from atoms and molecules to nanostructured materials. *Chem. Soc. Adv.*, **2020**, *49*, 6884.

[20] Peterson, A. A.; Nørskov, J. K. Activity Descriptors for CO_2 Electroreduction to Methane on Transition-Metal Catalysts. *J. Phys. Chem. Lett.*, **2012**, *3*, 251−258.

[21] Hori, Y.; Murata, A.; Takahashi, R. Formation of Hydrocarbons in the Electrochemical Reduction of Carbon Dioxide at a Copper Electrode in Aqueous Solution. *J. Chem. Soc.*, **1989**, *8*, 2309-2326.

[22] Kuhi, K. P.; Cave, E. R.; Abram, D. N.; Jaramillo, T. F. New insights into the electrochemical reduction of carbon dioxide on metallic copper surfaces. *Energy Environ. Sci.*, **2012**, 7050-7059.

[23] Jiang, K.; Sandberg, R. B.; Akey, A. J.; Liu, X.; Bell, D. C.; Norskov, J. K.; Chan, K.; Wang, H. Metal ion Cycling of Cu Foil for Selective C-C coupling in Electrochemical CO_2 Reduction. *Nature Catalysis*, **2018**, *1*, 111-119.

[24] Durand, W. J.; Peterson, A. A.; Studt, F.; Abild-Pedersen, F.; Norskov, J. K. Structure effects on the energetics of the electrochemical reduction of CO_2 by copper surfaces. *Surface Science*, **2011**, *605*, 1354-1359.

[25] Li, F.; Wang, Z.; Li, J.; Nam, D. H.; Lum, Y.; Luo, M.; Wang, X.; Ozden, A.; Hung, S. F.; Chen, B.; Wang, Y.; Wicks, J.; Xu, Y.; Li, Y.; Gabardo, C. M.; Dinh, C. T.; Wang, Y.; Zhuang, T. T.; Sinton, D.; Sargent, E. H. Cooperative CO_2-to-ethanol conversion via enriched intermediates at molecule–metal catalyst interfaces. *Nature Catalysis*, **2020**, *3*, 75-82

[26] Thao, T. H.; Verma, S.; Ma, S.; Fister, T. T.; Timoshenko, J.; Frenkel, A. I.; Kenis, P. J. A.; Gewirth, A. A. Nanoporous Copper−Silver Alloys by Additive-Controlled Electrodeposition for the Selective Electroreduction of CO_2 to Ethylene and Ethanol. *J. Am. Chem. Soc.* **2018,** *140***,** 5791-5797.

[27] Wei, X.; Yin, Z.; Luy, K.; Li, Z.; Gong, J.; Wang, G.; Xiao, L.; Lu, J.; Zhuang, L. Highly Selective Reduction of CO_2 to C2+ Hydrocarbons at Copper/ Polyaniline Interfaces. *ACS Catal.* **2020**, *10*, 4103-4111.

[28] Yan, T.; Guo, J. H.; Liu, Z. Q.; Sun, W. Y. Metalloporphyrin Encapsulation for Enhanced Conversion of CO_2 to C_2H_4. *ACS Appl. Mater. Interfaces.* **2021**, *13*, 25937-25945.

[29] Medal, M.; Wenzel C. Cu-Catalyzed Azide-Alkyne Cycloaddition. *Chem. Rev.* **2008**, *108*, 2952.

[30] Kang, D.; Hong Ko, J.; Choi, J.; Cho, K.; Lee, S. M.; Kim, H. J.; Ko, Y. J.; Park, K. H.; Son, S. U. Dual role of Cu_2O nanocubes as templates and networking catalysts for hollow and microporous Fe-porphyrin networks. **2017**, *17*, 2598-2601.

[31] Kutonova, K. V.; Trusova, M. E.; Postnikov, P. S.; Fillimonov, V. D.; Parello, J. A simple effective synthesis of aryl azydes via arenediazonium tosylates. *Synthesis.* **2013**, *45*, 2706-2710.

[32] Kang, D.; Ko, J. H.; Choi, J.; Cho, K.; Lee, S. M.; Kim, H. J.; Ko, Y. J.; Park, K. H.; Son, S. U. Hollow and microporous triphenylamine networks post-modified with TCNE for enhanced organocathode performance. *Chem. Commun.*, **2017**, *53*, 2598.

[33] Wang, M.; Torbensen, K.; Salvatore, D.; Ren, S.; Joulié, D.; Dumoulin, F.; Mendoza, D.; Lassalle-Kaiser, B.; Isci, U.; Berlinguette, C. P.; Robert, M. CO_2 electrochemical reduction with a highly active cobalt phthalocyanine. *Nature Communications*, **2019**, *10*, 3620.

[34] Kerour, A.; Boudjadar. S.; Bourzami, T.; Allouche, B. Eco-friendly synthesis of cuprous oxide (Cu_2O) nanoparticles and improvement of their solar photocatalytic activities. *J. Solid State Chem.*, **2018**, *263*, 79-83.

[35] Rapakousiou, A.; Shiotsuki, R.; Sakamoto, R.; Matsuoka, R.; Nakajima, U.; Pal, T.; Shimada, R.; Hossain, M. A.; Masunaga, H.; Horike, S.; Kitagawa, Y.; Sasaki, S.; Kato, K.; Ozawa, T.; Astruc, D.; Nishihara, H. Liquid/liquid interfacial synthesis of ‘’Click’’ Nanosheet. *Chem. Eur. J.*, **2017**, *23* (35), 8443-8449.

[36] Rahaman, N. S.; Ahmad, N. A. A.; Yhaya, M. F.; Azahari, B.; Ismail, W.R.; Crosslinking of fibers via azide–alkyne click chemistry: Synthesis and characterization. *J. App. Pol. Sci.*, **2016**, *25*, 45676.

[37] Weng, Z.; Jiang, J.; Wu, Y.; Wu, Y.; Guo, X.; Materna, K. L.; Liu, W.; Batista, V. S.; Brudvig, G. W.; Wang, H. Electrochemical CO_2 Reduction to Hydrocarbons on a Heterogeneous Molecular Cu Catalyst in Aqueous Solution. *J. Am. Chem. Soc.*, **2016**, *138* (26), 8076-8079.

[38] Kadish, K. M.; Bottomley, L. A.; Barce, J. G.; Winogard, N. X-ray Photoelectron Spectroscopic Studies on Monomeric and Dimeric Iron Porphyrins. *J. Am. Chem. Soc.* **1980**, *102* (13), 4341-4344.

[39] Möller, T.; Scholten, F.; Thanh, T.; Sinev, I. S.; Timoshenko, J.; Wang, X.; Jovanov, M. G.; Cuenya, B. R.; Varela, A. S.; Strasser, P.; Electrocatalytic CO_2 Reduction on CuOxNanocubes: Tracking theEvolution of Chemical State, Geometric Structure, and CatalyticSelectivity using Operando Spectroscopy. *Angew. Chem.,* **2020,** *41,* 18130-18139.

[40] Reske, R.; Mistry, H.; Behafraid, F.; Cuenya, B. R.; Strasser, P. Particle size effects in the catalytic electroreduction of CO_2 on Cu nanoparticles. *J. Am. Chem. Soc.*, **2014,** *136* (19), 6978-6986.